Atmos. Meas. Tech. Discuss., 8, 1401–1455, 2015
www.atmos-meas-tech-discuss.net/8/1401/2015/
doi:10.5194/amtd-8-1401-2015

Atmospheric Measurement Techniques Discussions

Use of the CALIOP vertical feature mask for evaluating global aerosol models

E. P. Nowottnick[1], P. R. Colarco[1], E. J. Welton[2], and A. da Silva[3]

[1]Code 614, NASA GSFC, Greenbelt, MD, 20771, USA
[2]Code 612, NASA GSFC, Greenbelt, MD, 20771, USA
[3]Code 610, NASA GSFC, Greenbelt, MD, 20771, USA

Received: 24 November 2014 – Accepted: 28 December 2014 – Published: 30 January 2015

Correspondence to: E. P. Nowottnick (edward.p.nowottnick@nasa.gov)

Published by Copernicus Publications on behalf of the European Geosciences Union.

Abstract

Global aerosol distributions provided by the NASA Modern Era Retrospective Analysis for Research and Applications aerosol reanalysis (MERRAero) are evaluated using the aerosol types identified by the CALIOP vertical feature mask (VFM) algorithm, focusing especially on Saharan dust distributions during July 2009. MERRAero is comprised of an aerosol simulation produced in the Goddard Earth Observing System version 5 (GEOS-5) Earth system model and incorporates assimilation of MODIS-derived aerosol optical thickness to constrain column aerosol loadings. For comparison to the CALIOP VFM we construct two synthetic VFMs using the MERRAero aerosol distributions: a Level 2 VFM in which simulated MERRAero total attenuated backscatter and estimated particulate depolarization ratios are input directly to the CALIOP VFM typing algorithm, and a Level 3 VFM in which we map the aerosol species in MERRAero to the CALIOP VFM types. By comparing the simulated MERRAero-Level 2 VFM to CALIOP VFM we can diagnose the aerosol transport and speciation in MERRAero. By comparing the MERRAero-Level 2 and MERRAero-Level 3 simulated VFMs we perform a simple Observing System Simulation Experiment (OSSE), which is useful for identifying shortcomings in the CALIOP VFM algorithm itself. We find that despite having our column AOT constrained by MODIS, comparison to the CALIOP VFM reveals a greater occurrence of dusty aerosol layers in our MERRAero-Level 2 VFM, due to errors in MERRAero aerosol speciation. Additionally, we find that the CALIOP VFM algorithm classification for desert dust and polluted dust should be reconsidered for aerosol features that contain dust mixtures in low aerosol loadings, as our application of the CALIOP VFM to MERRAero distributions flagged a greater presence of dusty vs. marine aerosols when our two MERRAero VFMs were compared.

AMTD
8, 1401–1455, 2015

1 Introduction

Mineral dust aerosols directly affect Earth's atmospheric radiative balance by absorbing and scattering light (Ryder et al., 2013; Balkanski et al., 2007; Zhu et al., 2007; Haywood et al., 2003; Tegen and Miller, 1998; Sokolik and Toon, 1996). Dust particles also act as cloud condensation (Kumar et al., 2009; Rosenfeld et al., 2001) and ice (Koehler et al., 2010; DeMott et al., 2003) nuclei, altering the microphysical properties – and, hence, radiative properties – of clouds, and modulating precipitation (Jenkins, 2008; Yoshioka et al., 2007; Rosenfeld et al., 2001). Furthermore, because of its radiative impacts, dust may affect tropical storm dynamics by enhancing atmospheric stability and inducing low-level wind shear that is not favorable for storm development (Reale et al., 2009, 2014; Dunion and Velden, 2004), with observational evidence suggesting that tropical storm activity and Saharan dust events are anti-correlated (Lau and Kim, 2007; Evan et al., 2006). Additionally, long-range transport and subsequent deposition of dust serves as a source of iron to terrestrial (Swap et al., 1992) and aquatic ecosystems (Mahowald et al., 2009), which in the latter case can enhance atmospheric CO_2 uptake by phytoplankton in iron-limited oceans (Jickells et al., 2005). Understanding of the roles of dust in all of these processes remains incomplete owing to the heterogeneous spatial, temporal, and compositional nature of dust and other related aerosols, and overall, aerosol interactions within the Earth system remain a driving source of uncertainty in assessing the current climate and projecting future climate (IPCC, 2014).

Global aerosol distributions are typically observed and quantified in terms of their optical properties, particularly aerosol optical thickness (AOT), a column measure of the aerosol loading. AOT is readily measured by ground-based sun photometers (e.g., the Aerosol Robotic Network, or AERONET (Holben et al., 1998)), and is a primary retrieval of space-based sensors such as those from the Moderate Resolution Imaging Spectroradiometer (MODIS, Remer et al., 2005; Levy et al., 2010) and the Multi-angle Imaging Spectroradiometer (MISR, Kahn et al., 2005). However, owing to spatial (e.g. AERONET) and temporal (e.g. MODIS) resolution limitations, as well as challenges in

AMTD
8, 1401–1455, 2015

isolating dust from the total aerosol loading, global aerosol transport models serve as useful tools to complement an incomplete observing system, by simulating the aerosol source, sink, and chemistry processes that impact the aerosol loading (Kim et al., 2014; Colarco et al., 2010; Textor et al., 2006; Kinne et al., 2006). Because of their high temporal and spatial resolution, the aerosol distributions simulated in aerosol data assimilation systems have the potential to fill in gaps in the existing observing systems. Global aerosol transport models may also be used to provide aerosol forecasts, which have numerous applications, ranging from air quality forecasts in the near term to simulating aerosol distributions for various climate scenarios on longer timescales. However, a significant limitation of global aerosol transport models is the need to characterize their uncertainties and errors (Huneuus et al., 2011; Textor et al., 2006; Kinne et al., 2006). Recently a number of modeling groups have adopted data assimilation capabilities to formally constrain the simulated AOT with observations from sensors such as MODIS (e.g., Sessions et al., 2014; Benedetti et al., 2009; Zhang et al., 2008). While a useful first order constraint, assimilation of single channel visible AOT observations do not correct uncertainty associated with speciation and vertical distributions of aerosols. Uncertainties in the speciation and vertical structure of aerosols has significant implications for characterizing aerosol transport pathways, quantifying loss processes, and understanding aerosol – Earth system interactions (e.g. impacts of aerosols on cloud lifetimes; aerosol radiative forcing) that are sensitive to the vertical location of specific types of aerosol.

Important information about the vertical distributions of aerosols has long been available from ground-based (Huang et al., 2010; Reid et al., 2003; Campbell et al., 2002; Welton et al., 2001, 2000) and airborne (Rogers et al., 2009; Reid et al., 2003; McGill et al., 2002; Browell et al., 1997, 1983) lidar systems, but by their nature these systems have limited spatial and temporal coverage. The launch of the space-based Cloud-Aerosol Lidar with Orthogonal Polarization (CALIOP) aboard the Cloud-Aerosol Lidar and Infrared Pathfinder Satellite Observations (CALIPSO) satellite on 28 April 2006, vastly increased the spatial and temporal coverage of aerosol and cloud vertical pro-

AMTD
8, 1401–1455, 2015

files (Winker et al., 2010). As part of NASA's "A-Train" (L'Ecuyer and Jiang, 2010) constellation of satellites, CALIPSO flies in formation with a number of other satellites, providing opportunities for coordinated multi-sensor retrievals of aerosol properties.

CALIOP provides daytime and nighttime attenuated backscatter profiles at 532 and 1064 nm, as well as information about depolarization at 532 nm. This information is first used to discriminate cloud and aerosol layers (Liu et al., 2005). Aerosol layers are then fed through a vertical feature mask (VFM) algorithm that assigns aerosol type classifications based on aerosol geographic location, the underlying surface type, and observed aerosol altitude, total attenuated backscatter, and depolarization ratio. The practical application of the CALIOP VFM is to assign an appropriate lidar ratio for each detected aerosol layer in order to compute aerosol extinction profiles from the attenuated backscatter signals, extinction being more directly comparable to model fields than backscatter (Omar et al., 2009). By itself, though, the VFM also provides a unique tool for directly exploring the vertical distribution of cloud and aerosol layers, as well as aerosol composition, but it's full potential has not yet been explored. Hagihara et al. (2010) and Yoshida et al. (2010) have used the cloud component of the VFM to determine the vertical distribution of ice and water clouds. Adams et al. (2012) and Chen et al. (2012) have used the aerosol component of the CALIOP VFM to classify the global three-dimensional distribution of specific aerosol types. Despite this utility, however, the VFM itself has never been comprehensively evaluated, and as far as we know there is no prior study that has used the VFM to evaluate three-dimensional distributions of aerosol type in the context of a global model at monthly timescales.

In this paper, we use the CALIOP VFM to evaluate aerosol speciation and vertical structure in MERRAero, a recently produced aerosol reanalysis based on the Modern Era Retrospective Analysis for Research and Applications (MERRA, Rienecker et al., 2011). MERRAero arises from a global aerosol simulation using the NASA Goddard Earth Observing System version 5 (GEOS-5) Earth system model assimilating AOT derived from the MODIS Terra and Aqua observations. Assimilation of AOT constrains the total aerosol loading in MERRAero, but not the aerosol speciation and ver-

AMTD
8, 1401–1455, 2015

tical structure. The model output aerosol mass and species distributions are subsequently sampled along the CALIOP ground-track, and we compute profiles of aerosol extinction and lidar observables (e.g., total attenuated backscatter, particulate depolarization ratio) using an offline lidar simulator. Two model-based VFM products are constructed from the profiles for comparison to the CALIOP VFM. The first product attempts to closely simulate the CALIOP VFM by simulating the CALIOP observables (e.g., total attenuated backscatter, estimated particulate depolarization ratio) from assimilated fields and feeding them directly into the CALIOP VFM algorithm (our so-called "MERRAero-Level 2" method). The second product is a model-derived VFM built by assigning aerosol type classification based on the individual species reported by MERRAero (our "MERRAero-Level 3" method). For a focused demonstration of the value of constructing our two synthetic MERRAero VFMs, we evaluate the July 2009 time period and the dust laden region over and downwind of the Sahara Desert. The objectives of our study are to evaluate the MERRAero aerosol vertical profiles and to investigate the CALIOP VFM-derived aerosol typing in comparison to the known typing information provided by GEOS-5. Our use of two different model-derived VFMs is meant to untangle algorithmic sensitivity embedded in the CALIOP VFM as well as understand the sensitivity of derived aerosol type to assumptions in our simulated aerosol optical properties (e.g., depolarization ratio). Furthermore, this work has implications for assessing the appropriateness of the CALIOP-assigned lidar ratios for extinction calculations. It also lays the groundwork for future lidar-based observing system simulation experiments (OSSEs) and supports new instrument development by simulating fundamental observables.

In Sect. 2, we describe the CALIOP instrument, its measurements, and the VFM product. In Sect. 3 we provide a description of the NASA GEOS-5 aerosol model, the MERRAero aerosol reanalysis, and provide an assessment of the MERRAero performance in terms of MODIS, MISR, and AERONET observation. In Sect. 4, we describe our methodology for evaluating MERRAero with the CALIOP VFM and how we con-

AMTD
8, 1401–1455, 2015

struct our model-derived VFMs using MERRAero assimilated fields. Our results are presented in Sect. 5 and in Sect. 6 we provide our conclusions.

2 The CALIOP instrument, feature detection, and vertical feature mask

2.1 The CALIOP instrument

CALIOP provides near-nadir vertical profiles of cloud and aerosol properties onboard the NASA CALIPSO satellite, flying in a sun-synchronous polar orbit in formation with a series of Earth observing systems in the so-called "A-Train." As an active sensor, CALIOP provides information both during the daytime (13:30 local equator crossing time) and nighttime (01:30 local equator crossing time) (Winker et al., 2006). CALIOP is a 2-wavelength lidar system, providing attenuated backscatter data at 532 and 1064 nm (Winker et al., 2006). Additionally, CALIOP is designed to provide polarization sensitive data at 532 nm to gain insight into particle shape (and cloud phase). These data include 532 nm profiles of parallel and perpendicular (relative to the laser polarization plane) attenuated backscatter. CALIOP makes measurements with a frequency of 20.16 Hz, yielding a horizontal resolution of 333 m at the Earth's surface (Winker et al., 2006). The vertical resolution of CALIOP varies, ranging from 300 m at the top of the CALIOP detection altitude (30.1–40 km) to 30 m within the typical altitude range where aerosols are observed near the Earth's surface (−0.5 to 8.2 km) (Winker et al., 2006). Daytime CALIOP observations are affected by solar background illumination, which decrease the signal-to-noise, making the daytime measurements more challenging to interpret. For our analysis we use CALIOP Version 3.01 data. For further information, including instrument specifications, we refer to Winker et al. (2006).

2.2 Feature detection

CALIOP Level 1B output includes profiles of attenuated backscatter at 532 and 1064 nm, and the perpendicular component of the backscatter signal at 532 nm (Winker

AMTD
8, 1401–1455, 2015

et al., 2006). This information is input to the CALIOP Level 2 algorithms, which are used to identify and classify cloud and aerosol layers, and retrieve extinction profiles (Vaughan et al., 2005; Liu et al., 2005). The attenuated backscatter is converted to a backscattering ratio, which is the ratio of the observed attenuated backscatter to what is expected in a purely molecular scattering profile. The CALIOP Level 2 feature finding algorithm searches the backscattering ratio profiles at the nominal 333 horizontal resolution for cloud and aerosol layers, identifying signals or features that are significantly greater than what is expected from the molecular-only profile (Vaughan et al., 2005). Features with strong backscatter ratios may require only a single lidar pulse for detection. However, fainter features often require horizontal averaging from anywhere from 5–80 km along-track to ensure detection in instances when the backscattering ratio is inhomogeneous, varying significantly along the track (Winker et al., 2006). Unfortunately, limitations of this averaging include potentially eliminating important spatial variability in the layer, and may result in cloud and aerosol features being averaged together. On the other hand, despite often requiring horizontal averaging for CALIOP Level 2 products, features identified in the vertical by CALIOP are often at horizontal resolutions finer than most global aerosol models, and so still provide a useful tool for evaluating the vertical location of aerosols in this model.

2.3 Vertical feature mask

Once a feature has been identified, the CALIOP algorithm utilizes the magnitude of attenuated backscatter and the color ratio $\chi = \beta_{1064}/\beta_{532}$, defined as the ratio of the attenuated backscatter at 1064 nm (β_{1064}) and 532 nm (β_{532}), to discriminate clouds from aerosols. Compared to aerosols, clouds exhibit enhanced attenuated backscatter values, so features with strong attenuated backscatter values are classified as cloud (Liu et al., 2005). Clouds also have larger particles compared to aerosols and at CALIOP wavelengths the attenuated backscatter is expected to be spectrally flat, and thus $\chi \approx 1$ (Liu et al., 2005). For aerosols, the attenuated backscatter at 1064 is expected to be

AMTD
8, 1401–1455, 2015

less than the attenuated backscatter at 532 nm, so features with $\chi < 1$ are classified as aerosol (Liu et al., 2005).

Once an observed feature has been detected and classified as an aerosol, the data are fed to the CALIOP Vertical Feature Mask (VFM) algorithm for further classification into aerosol type (Omar et al., 2009). The CALIOP algorithm assumes representative models of aerosol optical properties based on a multiyear cluster analysis of measurements made by the Aerosol Robotic Network (AERONET) of sun photometers (1993–2002) (Omar et al., 2005). The algorithm has models for six aerosol types or mixtures: dust, polluted continental, polluted dust, smoke, clean continental, and clean marine (Omar et al., 2009). Once an observed feature has been identified as aerosol, the attenuated backscatter at 532 nm is integrated between the feature base and top (Omar et al., 2009):

$$\gamma = \int_{z_{\text{top}}}^{z_{\text{base}}} \beta(z) T(z) \mathrm{d}z \tag{1}$$

where γ is the integrated total attenuated backscatter at 532 nm, β is the total (molecular + particulate) attenuated backscatter at 532 nm at altitude (z), and T is the total (molecular + particulate) atmospheric transmittance at altitude (z) (Omar et al., 2009).

Additionally, the volume (molecular + particulate) depolarization ratio at 532 nm is computed as the ratio of the perpendicular to parallel contributions to the total attenuated backscatter (Omar et al., 2009):

$$\delta_{\text{v}} = \frac{\sum_{z_{\text{base}}}^{z_{\text{top}}} \beta_{\perp}(z)}{\sum_{z_{\text{base}}}^{z_{\text{top}}} \beta_{\parallel}(z)} \tag{2}$$

AMTD
8, 1401–1455, 2015

where δ_v is the volume depolarization ratio of the feature at 532 nm, $\beta_\perp$ is the perpendicular attenuated backscatter signal at 532 nm at altitude (z), and $\beta_{||}$ is the parallel attenuated backscatter signal at altitude (z).

Using the volume depolarization ratio and assuming a molecular depolarization ratio of 0.0036 (Omar et al., 2009), the particulate depolarization ratio is estimated for input into the CALIOP VFM algorithm:

$$\delta_{ep} = \frac{\delta_v[(R-1)(1+\delta_m)+1] - \delta_m}{(R-1)(1+\delta_m)+\delta_m-\delta_v} \quad (3)$$

where δ_{ep}, δ_v, and δ_m are the estimated particulate, volume, and molecular depolarization ratios at 532 nm, respectively, and R is the mean ratio of the total attenuated backscatter to the molecular backscatter. It should be noted that Eq. (3) is the estimated particulate depolarization ratio and in order to obtain the actual particulate depolarization ratio, R is defined as the ratio of the total to molecular backscatter, not the ratio of the total attenuated backscatter (measured by CALIOP) to molecular backscatter. Defining R in this way leads to estimated particulate depolarization ratios that exceed the actual particulate depolarization ratio (Omar et al., 2009). In Sect. 4.2 where we describe our MERRAero-based based Level 2 VFM we are also using an estimated particulate depolarization ratio derived from a version of Eq. (3) to mimic the CALIOP VFM algorithm. We find that using the estimated particulate depolarization ratio vs. the actual particulate depolarization ratio has little impact on our aerosol tying.

Equations (1) and (3) are the calculated properties of the layer that are fed to the CALIOP Vertical Feature Mask (VFM) algorithm (see Table 1). Additionally, the VFM algorithm takes account of the layer altitude, location, elevation and underlying surface type in determining the aerosol type present. An elevated feature is identified if the lowest altitude of the feature begins 500 m above the Earth's surface or if the feature thickness is greater than 3 km (Liu et al., 2005). Surface types used in the CALIOP algorithm are from the International Geosphere – Biosphere Programme (IGBP) climatology (Loveland et al., 2000). The integrated total attenuated backscatter is used to

AMTD
8, 1401–1455, 2015

set the minimum backscatter threshold for identifying aerosol type over different land surface regimes in the CALIOP VFM algorithm. The estimated particulate depolarization ratio is used to identify non-spherical particles (e.g. dust) or mixtures that contain non-spherical particles (e.g. polluted dust). Surface type (e.g. snow or ice, desert, etc.), along with location and altitude (elevated vs. non-elevated aerosol layer) are also used to determine aerosol type in instances when mapping using observables alone is inconclusive. As an example, an elevated aerosol layer with a low particulate depolarization ratio over the Amazon would point to the smoke VFM flag. If the same aerosol layer extended to the surface, the VFM algorithm would point to the polluted continental flag. The CALIOP VFM aerosol types and logic pathways are illustrated in Table 1.

For our analysis, we use the six aerosol types identified in the CALIOP algorithm to validate our model: dust, polluted dust, polluted continental, clean continental, marine and smoke. Additionally, we include flags for clouds and signal attenuation (no signal), the Earth's surface, and instances when the algorithm cannot determine a cloud layer from an aerosol layer (Cloud – Aerosol Detection Failure) or when aerosol type is inconclusive (Aerosol Type Failure). For further information into the specifics of the CALIOP VFM algorithm, we refer to Omar et al. (2009).

3 The NASA GEOS-5 global aerosol transport model

3.1 GEOS-5 model description

GEOS-5 is an Earth system model and data assimilation system developed by the NASA Global Modeling and Assimilation Office (GMAO) that contains components for atmospheric circulation and composition, ocean circulation and biogeochemistry, and land surface processes coupled via the Earth System Modeling Framework (ESMF) (Hill et al., 2004). GEOS-5 is used for studying weather and climate variability, providing high quality meteorological and chemical analyses for NASA instrument teams and the scientific community. Along with traditional meteorological parameters (winds,

AMTD
8, 1401–1455, 2015

temperature, etc.) (Rienecker et al., 2008), GEOS-5 includes modules representing atmospheric composition, including aerosols (Colarco et al., 2010) and tropospheric/stratospheric chemical constituents (Pawson et al., 2008), and simulates the radiative impact of these constituents on the atmosphere.

GEOS-5 may be run at a range of spatial resolutions, from $2^\circ \times 2.5^\circ$ latitude by longitude to $\sim 3.5\,\text{km} \times 3.5\,\text{km}$ on a cubed sphere grid (Putman and Suarez, 2011). In the vertical, GEOS-5 has 72 levels on a hybrid-eta coordinate system that is terrain following near the surface transitioning to a pressure coordinate above 180 hPa, with a model top near 85 km. GEOS-5 may be run in a climate simulation mode, or in a data assimilation mode. For our simulations, we exploit the capability of GEOS-5 to run in replay mode, where rather than re-running the full meteorological data assimilation system, we replace the dynamical state of the system with a prior data assimilation run. In this analysis, we replay using the Modern Era Retrospective Analysis for Research and Applications (MERRA) (Rienecker et al., 2011) dataset, available every six hours at a spatial resolution of $0.5^\circ \times 0.625^\circ$.

Aerosols in GEOS-5 are treated with a version of the Goddard Chemistry, Aerosol, Radiation, and Transport (GOCART) model (Chin et al., 2002), which has been integrated into the GEOS modeling system as described in Colarco et al. (2010). GOCART treats five aerosol species (dust, sea salt, black carbon, organic carbon, and sulfate), including treatment of source and removal processes and chemistry. GOCART carries 5 size bins each of dust and sea salt, but otherwise simulates bulk mass of sulfate and carbonaceous aerosols, the latter of which is partitioned into hydrophobic and hydrophilic modes of black and organic carbon. The treatment of Saharan dust aerosols in particular has been evaluated in Nowottnick et al. (2010, 2011) and Colarco et al. (2014a). For all species except dust, aerosol optical properties are derived assuming Mie theory and refractive indices and growth factors primarily from the Optical Properties of Aerosols and Clouds (OPAC) database (Hess et al., 1998). For dust, we use an observation-derived set of refractive indices and assume a spheroidal particle shape distribution, following the methodology described in Colarco et al. (2014a) and

AMTD
8, 1401–1455, 2015

using the database of non-spherical dust optical properties from Meng et al. (2010). To represent aerosol scattering and extinction processes, we straightforwardly apply our aerosol optical properties lookup table to our simulated mass mixing ratios. This method should be distinguished from the CALIOP method of converting the backscatter to extinction via the lidar ratio. Our aerosol particulate depolarization ratios are determined from the Legendre polynomial moments of the polarized phase function in our aerosol optical property lookup tables and are weighted by each aerosol species contribution to scattering. Prior to our construction of our MERRAero VFMs, we found that our simulated particulate depolarization ratios are approximately 0.25 and lower than observed particulate depolarization ratios of 0.32 (Liu et al., 2008) and 0.31 (Freudenthaler et al., 2009) for Saharan dust events. We found that the optical properties in our look-up tables cannot reproduce the magnitude of observed particulate depolarization ratios for Saharan dust, most likely due to our inability to represent the actual non-sphericity of dust particles in our spheroid/ellipsoid particle models. Therefore, in attempt to match observed depolarization ratios (~ 0.31), we increase our simulated dust depolarization ratios by 30 % for our analysis. Finally, we note that non-spherical effects of dust are considered only for optical calculations and are not considered for transport or removal processes (e.g., sedimentation).

3.2 Aerosol data assimilation

Similar to our method of correcting the meteorological state using MERRA, we assimilate column AOT derived from MODIS instrument onboard the NASA Terra (launched 12 December 1999) and Aqua (launched 4 May 2002) satellites. This AOT assimilation algorithm involves cloud screening and homogenization of the observing system by means of a Neural Net scheme that translates cloud-cleared MODIS reflectances into AERONET calibrated AOT (referred to hereafter as "MODIS NNR"). Based on the work of Zhang and Reid (2006) and Lary et al. (2010) we originally developed a back-propagation neural network to correct observational biases in MODIS operational retrievals, but later evolved this system into a neural net type of retrieval. In this system,

AMTD
8, 1401–1455, 2015

reflectances (instead of retrievals) provide the main input, alongside solar and viewing geometry, MODIS cloud cover, climatological surface albedo and model derived surface wind speed. On-line quality control is performed with the adaptive buddy check of Dee et al. (2001), with observation and background errors estimated using the maximum likelihood approach of Dee and da Silva (1999). The AOT analysis in GEOS-5 is performed by means of analysis splitting. First, a 2-dimensional analysis of AOT is performed using error covariances derived from innovation data. The 3-dimensional analysis increments of aerosol mass concentration are computed using an ensemble formulation for the background error covariance. This calculation is performed using the Local Displacement Ensemble (LDE) methodology under the assumption that ensemble perturbations are meant to represent misplacements of the aerosol plumes. These ensemble perturbations are generated with full model resolution, without the need for multiple model runs. It is important to note that the single channel MODIS AOT observations does not have sufficient information content to constrain aerosol speciation and vertical structure, and the vertical structure of the analysis increments are determined by assumed error covariance.

The simulation of the global aerosol field in GEOS-5, driven by the MERRA atmospheric analyses and assimilating the MODIS-derived AOT is our so-called MERRAero aerosol reanalysis. MERRAero is performed at a horizontal spatial resolution of $0.5^{\circ} \times 0.625^{\circ}$ latitude-by-longitude and spans the time period from mid-2002 to the present. Applications of MERRAero are described in several recent papers, including Kessner et al. (2013), Buchard et al. (2014a, b), Colarco et al. (2014b), and Yasunari et al. (2014).

3.3 Evaluation of the MERRAero Saharan dust plume

In this section we provide an evaluation of the MERRAero simulated Saharan dust plume during July 2009 using space-based satellite imagery and lidar, and ground-based sun photometer observations. Figure 1 shows a comparison of the simulated monthly mean AOT over the Sahara Desert and the tropical North Atlantic Ocean

AMTD
8, 1401–1455, 2015

to several satellite derived AOT products. Observations from MISR (Fig. 1b) provide AOT retrievals at 558 nm under cloud-free conditions, combining information from nine differently angled push-broom cameras that observe the same scene on Earth over a period of seven minutes. Owing to this multi-angle viewing geometry, MISR is able to provide retrievals over bright surfaces (Diner et al., 1998; Abdou et al., 2005), with additionally some insight into particle size, shape, and composition. The MISR swath width along the ground is about 360 km, providing global coverage approximately every nine days. MISR Level 2 AOT values from the latest version of the MISR aerosol retrieval algorithm (v. F12_0022) are used at 558 nm. In addition to MISR, we show the standard Collection 5.1 (Fig. 1c) retrieval from MODIS Aqua, providing near-daily coverage at 10 km × 10 km spatial resolution. Operationally, MODIS retrieves AOT under cloud free conditions using reflectances at six visible channels over ocean (Tanré et al., 1997), and over dark land surfaces using two visible and one near-IR channel (Kaufman et al., 1997; Levy et al., 2007a, b). Aerosols are not retrieved over bright desert surfaces in the standard "dark target" land algorithm. We also show the MODIS NNR assimilated in MERRAero (Fig. 1d). For our evaluation, we have regridded all satellite observations to the GEOS-5 grid using a simple box averaging approach.

For a consistent comparison between MISR and GEOS-5, we sample our GEOS-5 AOT at the model grid cell that contains the MISR observation at the nearest hourly output time. Compared to MISR, MERRAero captures the general position and AOT magnitude of the observed Saharan dust plume emerging from North Africa and carried toward the Caribbean. Over the Caribbean, however, the AOT magnitude of the plume is slightly underestimated in MERRAero when compared to MISR, potentially due to cloud contamination in the MISR aerosol retrieval over the ocean (Shi et al., 2014). Over North Africa, peak AOT values are observed by MISR over Lake Chad and Mali, and these AOT values are greater than what is simulated in MERRAero. For comparison, the standard Collection 5.1 MODIS AOT product (Fig. 1c) shows a much fuller picture of the Saharan aerosol plume, reflecting the greater spatial coverage relative to MISR, except over the oceans. The monthly mean MODIS NNR AOT (Fig. 1d)

AMTD
8, 1401–1455, 2015

is most like MERRAero, which is natural as that was the product assimilated. Note that the quality screening of the MODIS data used to compile the NNR AOT results in a lower AOT over the Caribbean than in either the MODIS Collection 5.1 or MISR AOT products.

We also compare MERRAero to AERONET observations in order to evaluate the timing and magnitude of simulated AOT and Angstrom Exponent (AE). This is done for several stations near and downwind of the source region (Fig. 1a). AERONET provides measurements of AOT using direct solar extinction measurements at 340, 380, 440, 500, 670, 870, and 1020 nm, with 15 min temporal resolution (Holben et al., 2001). We use quality-assured and cloud-screened (Level 2) hourly AERONET AOT values (Smirnov et al., 2000) for comparison to MERRAero. AE is a measure of the dependence of AOT on wavelength, which is a function of particle size (Eck et al., 1999). Larger particles like dust typically exhibit AE values less than 1, while smaller particles have AE values greater than 1 (Eck et al., 1999).

Figure 2a compares AOT and AE values between AERONET hourly observations and corresponding MERRAero values for two stations near the Saharan source region. At Capo Verde, an island site off the west African coast and under the main dust pathway, MERRAero captures the timing and observed magnitude of AOT during July with a modest correlation coefficient (r^2 = 0.437), though there is little to no quality assured data to evaluate the high AOT events simulated in MERRAero. AE values observed by AERONET at Capo Verde are predominantly less than 1, indicating the presence of dust aerosols (Fig. 2a). Comparatively, MERRAero AE values are less than 1 and not well correlated (r^2 = 0.209) when compared to those observed by AERONET, indicating that we are simulating aerosols that are too small due to an incorrect representation of the dust particle size distribution or too large of a contribution from anthropogenic aerosols, such as biomass burning at this location. On the northern edge of the dust plume, at Santa Cruz, Tenerife, MERRAero is more comparable to the observed AOT magnitude and time series (r^2 = 0.707), and accurately captures the passage of several high AOT events in the latter part of the month (Fig. 2a). Similar to Capo Verde,

AMTD
8, 1401–1455, 2015

both AERONET and MERRAero AE values are predominantly less than 1 (r^2 = 0.685), though the model is again slightly biased high throughout the month.

Downwind of the source region (Fig. 2b) at Camaguey, Cuba, MERRAero captures the timing of transported aerosol events (r^2 = 0.589), but generally simulates lower AOT magnitudes for specific events when compared to AERONET. AERONET and MERRAero AE values at Camaguey are again predominantly less than 1 and anti-correlated with their respective AOT values, properties indicative of Saharan dust transport. Comparing MERRAero to AERONET AE values, they are only moderately correlated with each other at Camaguey (r^2 = 0.503) and simulated values are greater than those observed by AERONET. At La Parguera, Puerto Rico, MERRAero accurately simulates the timing and magnitude of AOT (r^2 = 0.828), though consistent with our comparison at Camaguey, MERRAero AE values are slightly biased high when compared to AERONET and are moderately correlated (r^2 = 0.584).

In Fig. 3 we illustrate the impact of CALIOP aerosol typing on the extinction by comparing the monthly mean MERRAero dust vertical extinction profiles to those determined by CALIOP. By using aerosol layers identified as dust by the CALIOP VFM, the observed backscatter signal can be converted to extinction using the lidar ratio and the dust extinction may be separated from the total extinction. In Fig. 3, CALIOP extinction data are from their monthly Level 3 gridded (5° longitude × 2° latitude) product, and the MERRAero dust extinction is sampled along the CALIPSO track and across desert dust features observed by CALIOP at several longitudes moving westward from the Saharan dust source region. Over the source region, at 7.5° W, MERRAero simulates peak dust extinction values at the same latitudes as observed by CALIOP, but with the dust confined to lower altitudes. We note again that there are no MODIS-derived AOT to assimilate over bright surfaces such as the Saharan source region, which would impact simulated dust plume position and timing, potentially influencing the simulated vertical aerosol distribution when sampled coincident with CALIOP dust features. Moving to the west at 27.5° W (in the tropical Atlantic, west of Capo Verde), MERRAero accurately captures the magnitude of the elevated (2–5 km altitude) dust over the tropical North

AMTD
8, 1401–1455, 2015

Atlantic Ocean, though the model does not simulate peak high extinction values below 1 km. Further to the west at 47.5° W, MERRAero again captures observed extinction magnitudes and elevation when compared to CALIOP. Once again the high extinction values observed by CALIOP at altitudes below 1 km are not found in the MERRAero simulation.

Figure 3 shows that MERRAero is able to capture the CALIOP retrieved elevated dust layers, but not the features seen in CALIOP at low altitudes. The low level "dust" features seen in the Level 3 CALIOP extinction product highlight the importance of identifying the correct aerosol type in the VFM, as it is central to identifying these features as dust, and hence assigning a dust-appropriate lidar ratio to compute extinction. Misidentification of the feature as dust instead of, say, marine, could explain these features. In Fig. 3, we also include the MERRAero seasalt extinction and we see correspondence between low-level MERRAero seasalt and low-level CALIOP dust. However, it is also possible that model is simply missing the presence of low-level dust layers over the tropical North Atlantic.

4 Methodology for constructing MERRAero vertical feature masks and application to a case study

Here we use as an example the CALIOP sampled nighttime aerosol profile (0Z–1Z) across North Africa on 7 July 2009 (Fig. 4a) to illustrate the CALIOP VFM product and our two synthetic vertical feature masks derived from the MERRAero simulated aerosol fields. The first of our model-derived VFMs is our MERRAero-Level 2 method, in which we compute the total attenuated backscatter and estimated particulate depolarization ratio (see Eq. 3) profiles based on the MERRAero fields, and provide those as inputs to the CALIOP VFM algorithm discussed in Sect. 2.3. Our second model-derived VFM is our MERRAero-Level 3 method, in which we map the simulated MERRAero aerosol composition distributions to the types identified by the CALIOP VFM based on the simulated speciated extinction. In practice, our MERRAero-Level 3 method is limited in

AMTD
8, 1401–1455, 2015

that we are not simulating exactly the aerosol classifications specified in the CALIOP VFM, so this method has some subjectivity associated with it. By constructing two MERRAero derived VFMs in this manner, we identify two distinct objectives. First, by comparing the MERRAero-Level 2 VFM to the observed CALIOP VFM, we can identify biases in MERRAero aerosol speciation and transport. Then, by comparing our two entirely synthetic MERRAero VFMs, we can document the ability of the CALIOP VFM algorithm to properly identify aerosol types and identify shortcomings of the algorithm itself.

4.1 Sampling MERRAero

As mentioned in Sect. 2, the CALIOP feature finding algorithm looks for enhanced attenuated scattering ratio profiles to differentiate aerosol and cloud features from molecular backscatter. For a given column, up to 8 layer features are permitted in the detection algorithm. For sampling MERRAero along CALIOP aerosol features, we use the 5 km Level 2 CALIOP layer product, which provides feature vertical thickness and location at 5 km spatial resolution.

We sample MERRAero at the location of each aerosol feature in the 5 km Level 2 CALIOP layer product so there is a direct correspondence between CALIOP aerosol features and the MERRAero model fields that are used to construct the MERRAero-Level 2 and MERRAero-Level 3 VFMs. We then regrid all VFMs to the GEOS-5 grid by taking the mode value (VFM flags are qualitative and cannot be averaged, hence the most frequent feature type is used) in the altitude, latitude, and longitude range of a GEOS-5 grid box.

4.2 The MERRAero level 2 method: application of the CALIOP VFM algorithm to MERRAero

For our first method, we simulate from the MERRAero aerosol mass fields the profile of 532 nm total attenuated backscatter, including both the particulate and molecular

AMTD
8, 1401–1455, 2015

(Rayleigh) scattering components and compute the estimated particulate depolarization ratio that is used by the CALIOP VFM algorithm. To reiterate, the particulate 532 total attenuated backscatter is computed by application of our aerosol optical properties lookup tables (Sect. 3.1) to the simulated mass mixing ratios. In order to account for the molecular contribution to our simulated total attenuated backscatter, we follow Russell et al. (1993) to parameterize the Rayleigh backscatter coefficient and molecular optical thickness. We then construct the total attenuated backscatter signal by adding the particulate and molecular backscatter coefficients multiplied by the particulate and molecular two-way transmittances. Because the estimated particulate depolarization ratio and not the actual particulate depolarization ratio is fed into the CALIOP VFM algorithm, we compute the estimated particulate depolarization ratio from our actual particulate depolarization ratio using Eq. (3). We again note that the estimated particulate depolarization ratio is greater than the actual particulate depolarization ratio, however, we find that this has little impact on our aerosol typing in our MERRAero-Level 2 VFM (not shown).

On 7 July 2009 CALIPSO flew southwesterly beginning over Russia, over northeastern Africa, across Central Africa, south to the southeastern corner of Africa (Fig. 4a). In the model we see this track crossing several different aerosol regimes, and the total extinction profile (Fig. 4b) shows several distinct features and plumes of different depths (labeled A, B, and C). The CALIOP total attenuated backscatter and volume depolarization ratio (averaged to 5 s) for this case study are shown in Fig. 4e and f, respectively. In Fig. 4c and d, MERRAero total attenuated backscatter and estimated particulate depolarization ratio are shown. Comparing the MERRAero and CALIOP total attenuated backscatter (Fig. 4c and e), we see the MERRAero profile is mostly comparable to CALIOP, showing an aerosol layer from the surface to about 4 km altitude over Eastern Europe and Turkey (Fig. 4b – feature A), followed by an aerosol layer with a top varying in altitude between 2–6 km that corresponds to high AOT over North Africa (Fig. 4b – feature B), and finally an optically thick aerosol layer over Central Africa extending to 4 km (Fig. 4b – feature C). Comparing the depolarization ratios profile along the track

AMTD
8, 1401–1455, 2015

(Fig. 4d and f), MERRAero is comparable to CALIOP, showing volume depolarization ratio values ranging from 0.1 to beyond 0.2 over North Africa (feature B), which is indicative of dust aerosols, although the MERRAero values extend to higher altitudes when compared to CALIOP for this case study. Comparing MERRAero extinction to the estimated depolarization ratio, we see that this bias occurs in regions with low dust loadings, which would likely be below the detection limits of CALIOP. The depolarization ratio for the aerosol feature over Central Africa is near zero in both CALIOP and MERRAero (feature C), a signature of spherical aerosols such as aged smoke. Further exploration (not shown) reveals this feature is primarily comprised of carbonaceous aerosol, suggesting that the feature is related to biomass burning.

For each aerosol feature identified in the Level 2 CALIOP layer product, we first require a minimum simulated 532 nm MERRAero extinction threshold of 0.003 km^{-1}, which corresponds to the CALIOP minimum detectable signal for marine aerosol at night, at 1 km altitude, and for maximum feature horizontal averaging (80 km) (Winker et al., 2013). We select marine aerosol for our minimal extinction threshold, as it has the smallest lidar ratio and therefore for a given backscatter in an aerosol layer, marine aerosol will have the lowest corresponding extinction and is thus the most conservative extinction threshold choice. We implement this requirement to prevent flagging MERRAero aerosol layers that would not be detected by CALIOP. If the minimum extinction threshold is not met, the feature will be flagged as clear in the MERRAero-Level 2 VFM.

Next, the MERRAero total attenuated backscatter and estimated particulate depolarization ratios are calculated across the feature altitude using Equations 1 and 3, and, along with IGBP surface type and feature altitude, are then fed to the VFM algorithm in Table 1 to assign one of the six CALIOP aerosol types. By applying the CALIOP VFM in this way, there is a direct correspondence between aerosol layers identified by CALIOP and those sampled in MERRAero to construct a comparable VFM.

If CALIOP does not identify an aerosol layer, MERRAero will not be sampled in the model. In this method, MERRAero is only sampled where CALIOP identifies an aerosol

AMTD
8, 1401–1455, 2015

feature and if the aerosol layer exceeds our minimal extinction threshold, one of the six aerosol types in Table 1 will be flagged to construct the MERRAero-Level 2 VFM.

4.3 The MERRAero level 3 method: constructing a VFM from MERRAero fields

As an alternative to the direct simulation of the CALIOP VFM from a MERRAero CALIOP simulator as described above, we have also constructed a VFM that maps the aerosol types explicitly simulated in MERRAero to the aerosol types in the CALIOP VFM. In this way, the MERRAero-Level 3 VFM provides a CALIOP – like VFM that is representative of the aerosols simulated in MERRAero. We recall that there are five aerosol types simulated in MERRAero (dust, sea salt, black carbon, organic carbon, and sulfate). For simplicity of type assignment we aggregate the black and organic carbon together to be a single carbonaceous species, which is practically used to assign aerosol types to the CALIOP "smoke" classification (see below, and Table 2).

The first step in this MERRAero-Level 3 MERRAero classification algorithm is the same as in the MERRAero-Level 2 method. For this algorithm we still sample the model where CALIOP identifies an aerosol feature. For each aerosol feature identified by CALIOP, we compute the extinction of the corresponding layer in MERRAero and check to see if the minimum total extinction threshold requirement is met. If our threshold ($0.003\,km^{-1}$) requirement is met, we determine the individual extinction for each of the simulated aerosol types over the feature altitude range. Because we consider 4 independent aerosol types in MERRAero (dust, sea salt, sulfate, and carbon), we consider the presence of a specific aerosol to be significant if it contributes at least 25 % of the total extinction across a feature. For example, if the total extinction across a feature is greater than $0.003\,km^{-1}$ and dust and carbon each contribute $> 25\,\%$ to the feature signal, then both dust and carbon would be flagged as being present. In our MERRAero-Level 3 method, it is possible that extinction values will not meet threshold criteria, and so our aerosol typing can be flagged as clear even where CALIOP identified a layer.

AMTD
8, 1401–1455, 2015

A major challenge in constructing a VFM using MERRAero fields lies in relating the aerosol types simulated by the model to the aerosol types provided by the CALIOP VFM, as we do not explicitly simulate the mixtures of aerosols that are flagged by the CALIOP VFM (e.g. polluted dust). Our mapping to the CALIOP VFM aerosol types and the minimal fraction of each MERRAero aerosol type for each CALIOP aerosol type is laid out in Table 2. Some of the MERRAero to CALIOP VFM mapping is straightforward, such as desert dust, but in other cases – specifically those related to polluted aerosol types – the typing criteria are more subjective. For example, in grid cells where dust, sea-salt, or sulfate aerosol meet the total extinction threshold and are the only aerosol types to contribute at least 25 % to the total extinction signal, these cells are mapped directly to the desert dust, marine, and clean continental CALIOP VFM flags, respectively. The CALIOP Algorithm Theoretical Basis Document (ATBD) (Liu et al., 2005) indicates that the polluted continental flag could be representative of a sooty sulfate aerosol. Therefore, we map our MERRAero carbon + sulfate mixtures to the polluted continental CALIOP VFM flag. Similarly, the CALIOP algorithm indicates that the polluted dust flag is representative of a dust + smoke or a dust + sulfate mixture. In practice, CALIOP identifies any dust + other aerosol mixture as polluted dust (Omar et al., 2009). Therefore, to be consistent with CALIOP, any feature where dust contributes to at least 25 % of the total extinction is mapped to polluted dust. For our aforementioned hypothetical feature that meets the extinction threshold criteria and both dust and carbon contribute each to > 25 % of the extinction signal, the feature would be identified as polluted dust using the MERRAero-Level 3 method (Table 2).

In Table 3 we compare 532 nm lidar ratios (S_a) and single scattering albedos (SSA) from our average MERRAero-Level 3 mapping of MERRAero aerosols to CALIOP aerosol types to CALIOP values derived by applying Mie theory to the physical and optical properties of the CALIOP aerosol models (Table 1 from Omar et al., 2009). Comparing the MERRAero and CALIOP S_a and SSA values, there are notable differences in the clean continental and polluted dust S_a, as well as the polluted dust SSA. These differences are directly related to the challenge of mapping MERRAero aerosols

AMTD
8, 1401–1455, 2015

to the CALIOP aerosol types. The higher MERRAero clean continental Sa value is the result of mapping MERRAero sulfate aerosols to the background clean continental CALIOP aerosol type. Similarly, by mapping any dust mixture to the polluted dust type, our polluted dust S_a and SSA values also include dust mixtures with highly scattering aerosols such as sea salt that result in a lower S_a and higher SSA when compared to the CALIOP polluted dust model. Overall, however, there is good agreement between MERRAero and CALIOP S_a and SSA values, indicating that our MERRAero-Level 3 methodology leads to an adequate representation of the CALIOP aerosol types.

4.4 A VFM case study on 7 July 2009

Figure 5 shows the CALIOP and two MERRAero VFMs for the orbital track shown in Fig. 4a on 7 July 2009. Here, the CALIOP VFM identified a layer of polluted dust over Turkey (feature A in Fig. 4a), primarily located between 2–5 km in altitude, followed by a low layer of marine aerosol over the Mediterranean Sea (Fig. 5a). Moving south over North Africa, polluted dust is detected by the CALIOP VFM at altitudes below 2–3 km near the coastline, transitioning to desert dust near 23° N at altitudes to 3–5 km and extending south to 8° N over North Africa (Fig. 4a – feature B). South of 8° N, the CALIOP VFM transitions from desert dust to polluted dust, as this is a region where Saharan dust aerosols frequently interact with smoke aerosols from biomass burning to the south. Continuing south of 5° N over Central Africa (Fig. 4a – feature C), smoke aerosols are the dominant aerosol type in the CALIOP VFM (Fig. 5a).

By comparing the CALIOP VFM (Fig. 5a) to our MERRAero-Level 2 VFM (Fig. 5b), we can identify biases in simulated aerosol speciation and transport in MERRAero by identifying instances where the CALIOP and the MERRAero-Level 2 method aerosol typing differ. Over Turkey, the MERRAero-Level 2 method flags a mixture of polluted dust, desert dust, and smoke as the dominant aerosol types and compares well with CALIOP. However, over the Mediterranean Sea, our MERRAero-Level 2 VFM is predominantly polluted dust vs. marine, suggesting that MERRAero is transporting dust into a region that was observed to be relatively dust free by CALIOP. Our MERRAero-

AMTD
8, 1401–1455, 2015

Level 2 VFM (Fig. 5b) does not capture this transition and instead flags desert dust as the predominant aerosol type over North Africa. Additionally, the observed transition of polluted dust to smoke in the CALIOP VFM occurs further to the north in the MERRAero-Level 2 VFM, suggesting that MERRAero is not simulating dust as far south as observed by CALIOP. South of 5° N, our MERRAero-Level 2 VFM is comparable to the CALIOP VFM by indicating smoke as the dominant aerosol type.

By comparing our MERRAero-Level 2 (Fig. 5b) and MERRAero-Level 3 (Fig. 5c) VFMs, we can assess CALIOP VFM algorithm for this case. Over Turkey, our MERRAero-Level 2 and MERRAero-Level 3 VFMs differ, as the MERRAero-Level 3 VFM flags a reduced presence of dust and a greater presence of polluted continental aerosols. This highlights that the CALIOP VFM algorithm has difficulty properly identifying aerosol type for aerosol layers with low estimated particulate depolarization ratios (i.e. polluted dust), as while there was sufficiently enough dust in MERRAero to classify the aerosol layer as polluted dust in terms of the estimated particulate depolarization ratio in the MERRAero-Level 2 VFM, comparison to our MERRAero-Level 3 VFM reveals a lesser presence of dust and a greater contribution polluted continental (smoke + sulfate) aerosols. Over the Mediterranean Sea, our MERRAero-Level 2 and 3 VFMs agree in terms of not flagging as much marine aerosol as observed by CALIOP but differ in terms of type, as our MERRAero-Level 3 VFM indicates a transition of dust to continental aerosol, while our MERRAero-Level 2 VFM is dominated by polluted dust. South of the Mediterranean Sea, our MERRAero VFMs agree with one another and match the transition of desert dust over North Africa to polluted dust over the Sahel, followed by smoke over Central Africa.

In this case study, we have demonstrated the utility of constructing two different VFMs for identifying biases in simulated MERRAero vertical aerosol distributions by comparing our MERRAero-Level 2 VFM to the CALIOP VFM, as well as establishing limitations of the CALIOP VFM algorithm by comparing our MERRAero-Level 2 and MERRAero-Level 3 VFMs. In next section, we extend our analysis to include all of July 2009 to

AMTD
8, 1401–1455, 2015

quantify biases in MERRAero vertical aerosol distributions and optical properties, as well as the CALIOP VFM algorithm on a longer timescale.

5 Monthly application of VFM for July 2009

In this section, we extend our evaluation of the vertical aerosol distributions in our MERRAero aerosol reanalysis by applying both of our MERRAero VFM methodologies for comparison to the CALIOP VFM for July 2009. For our monthly analysis, we perform our sampling of MERRAero as described in Sect. 4.1 and bin all CALIOP and MERRAero VFMs on the $0.5^\circ \times 0.625^\circ$ MERRAero grid. Due to the narrow swath of the CALIOP instrument, many grid boxes on the model's grid are devoid of observations at the monthly timescale. Accordingly, in order to produce maps relatively devoid of observational gaps we regrid the CALIOP and MERRAero VFMs to a coarser $1^\circ \times 1.25^\circ$ spatial resolution, maintaining the most frequent type classification as the grid box value. After this regridding, the number of observations within each grid box during a month becomes more uniform, with most tropical grid boxes containing 4–8 observations at each altitude bin. Within in each grid box, we find the mode, as well as determine the fraction of occurrence of VFM type to understand the variability of aerosol type during the month. In an effort to evaluate observed aerosols in cloudy environments, we only consider the aerosol component of the CALIOP VFM for our monthly analysis. For our monthly analysis, we combine both CALIOP day and night VFM files, as we did not see a significant impact on VFM typing and sampling when they were treated separately (not shown).

Figure 6 shows the July 2009 CALIOP VFM at 1 km vertical intervals over North Africa, the tropical North Atlantic, and the Caribbean. Between 0–1 km, the CALIOP VFM is dominated by desert dust over most of North Africa. We note the presence of marine aerosol over North Africa in the CALIOP data. However, we suspect this feature is an error in the VFM. Downwind of the source region, we see a mixture of marine and polluted dust extending into the Caribbean between 10–20° N. In the Caribbean, we

AMTD
8, 1401–1455, 2015

see a frequent occurrence of polluted dust, which extends over into the Eastern Pacific. Moving up to 1–2 km, North Africa is again dominated by desert dust and we see a greater fraction of polluted dust vs. marine aerosol downwind of the source region associated with dust transport as part of the lofted Saharan Air Layer (SAL). Over the Caribbean and Eastern Pacific, we again see a mixture of polluted dust and marine aerosol. Between 2–3 km and 3–4 km, North Africa remains dominated by desert dust, and we see an increased fraction of polluted and desert dust with altitude both downwind of the source region and over the Caribbean/Eastern Pacific associated with dust laden SAL transport. We also begin to see more regions where the grid cells are identified as clear in the CALIOP VFM, where no aerosol layers were detected throughout the month. Continuing upward to 4–5 and 5–6 km, aerosol layers are less common, but we continue to see desert dust over North Africa and a large fraction of desert and polluted dust downwind over the tropical North Atlantic. However, over the Caribbean, while both desert and polluted dust flags are present, there are relatively fewer grid boxes that contain dust aerosols at 5–6 km when compared to the tropical North Atlantic and North Africa, related to dust removal during transport from Saharan source region to the Caribbean.

Figure 7 shows the July 2009 MERRAero-Level 2 VFM. To reiterate, by comparing the MERRAero-Level 2 VFM (Fig. 7) to the CALIOP VFM (Fig. 6), we can assess biases in our simulated dust transport. Over the Saharan source region, the MERRAero-Level 2 VFM flags desert dust over central North Africa and is in agreement with the CALIOP VFM at all altitude ranges. Over the tropical North Atlantic Ocean between 0–1 km, the MERRAero-Level 2 VFM flags a mixture of desert and polluted dust and is comparable to the CALIOP VFM. However, at 1–2 km and above, the MERRAero-Level 2 VFM flags a broader dust plume that extends significantly farther north and south when compared to the CALIOP VFM, suggesting that dust transport is too liberal in MERRAero. Additionally, on the periphery of the transported Saharan dust plume, the MERRAero-Level 2 VFM flags significantly more aerosol layers as polluted dust in the transition from desert dust to marine aerosol, which is not seen in the CALIOP VFM. We recall that

AMTD
8, 1401–1455, 2015

in MERRAero the fraction of each individual aerosol species does not change when MODIS AOT is assimilated. Therefore, if the fraction of dust relative to other aerosol species is incorrect, this bias will be preserved after MODIS AOT is assimilated. Over the Caribbean and East Pacific Ocean, the CALIOP and MERRAero-Level 2 VFMs are comparable at 0–1 km, flagging a mixture of desert dust, polluted dust, and marine aerosol. Above 1 km, our MERRAero-Level 2 VFM flags a greater presence of desert dust and polluted dust when compared to the CALIOP VFM. This difference persists into the East Pacific, suggesting that in addition to simulating a much broader Saharan dust plume, MERRAero transports dust too far west when compared to CALIOP.

Figure 8 shows the July 2009 MERRAero-Level 3 VFM. By comparing our MERRAero-Level 3 (Fig. 8) and MERRAero-Level 2 VFMs (Fig. 7), we can assess the performance of the CALIOP VFM algorithm. Over the Saharan source region, both of our MERRAero VFMs are in agreement and flag desert dust as the dominant aerosol type. Over the tropical North Atlantic at 0–1, 1–2, and 2–3 km, the MERRAero-Level 3 VFM flags a narrower plume of desert dust mixed surrounded by polluted dust (dust + sea-salt) that compares more favorably to the CALIOP VFM than our MERRAero-Level 2 VFM. Comparing our MERRAero VFMs, we see that the MERRAero-Level 2 VFM dust plume is broader than the MERRAero-Level 3 VFM over the tropical North Atlantic, suggesting that using the estimated particulate depolarization ratio alone in the CALIOP VFM algorithm potentially flags aerosol layers as dusty when the actual dust aerosol loading is small. Above 3 km, the MERRAero-Level 2 VFM continues to flag a broad region of desert dust and polluted dust aerosol, while the MERRAero-Level 3 VFM aerosol flags are very comparable to CALIOP. Over the Caribbean and Eastern Pacific, our MERRAero-Level 3 VFM slightly differs from the MERRAero-Level 2 and CALIOP VFMs and flags more marine aerosol pixels at the expense of desert and polluted dust. At 1–2 km, our MERRAero-Level 2 VFM is dominated by desert and polluted dust, while our MERRAero-Level 3 VFM flags a mixture of desert dust, polluted dust, and marine aerosol. At 3 km and beyond, our MERRAero-Level 3 VFM flags fewer dusty aerosol layers with altitude, while our MERRAero-Level

AMTD
8, 1401–1455, 2015

2 VFM continues to flag desert dust and polluted dust over the Caribbean and East Pacific. This feature again suggests that using the estimated particulate depolarization ratio alone is too permissive for flagging dust layers in the CALIOP VFM algorithm, particularly in regions where the low aerosol loading is low and multiple aerosol types are present.

To reiterate, Figs. 6–8 all show the mode aerosol type for July 2009, as VFM flags are not quantitative and cannot be averaged. Therefore, in Fig. 9, we show the fraction of occurrence for each VFM flag over the tropical North Atlantic (0–30° N, 60–15° W, Fig. 9a) and the Caribbean/East Pacific (0–30° N, 110–60° W, Fig. 9b). Over the tropical North Atlantic, we again see that the our MERRAero-Level 2 VFM flags a significantly greater occurrence of desert dust and polluted dust at the expense of marine aerosol layers when compared to the CALIOP VFM, reaffirming that too much dust is being transported downwind in MERRAero. Our MERRAero-Level 3 VFM is comparable to the CALIOP VFM over the tropical North Atlantic, however, when we compare our MERRAero-Level 2 and MERRAero-Level 3 VFMs, we clearly see that the CALIOP VFM algorithm flags a greater occurrence of desert and polluted dust in regions that are not identified as dusty in our MERRAero-Level 3 VFM. These features persist over the Caribbean/East Pacific, as we again see a greater occurrence of desert dust and polluted dust at the expense of marine aerosol in our MERRAero-Level 2 VFM when compared to the CALIOP and MERRAero-Level 3 VFMs.

6 Conclusions

In this study, we have explored the utility of the CALIOP VFM for evaluating Saharan dust transport for July 2009 in the NASA GEOS-5 aerosol reanalysis (MERRAero). The CALIOP VFM is particularly used for evaluating global aerosol transport models, as the VFM provides information regarding vertical location and aerosol type, which is challenging to assess using traditional column measurements of AOT such as MODIS.

AMTD
8, 1401–1455, 2015

For our analysis, we first evaluated Saharan dust in our 0.5° × 0.625° MERRAero simulation for July 2009. Compared to column AOT observations from MISR, MODIS-Aqua, and AERONET, we showed that MERRAero simulated the magnitude and timing of observed Saharan dust events during July 2009. Vertically, when compared to the CALIOP Level 3 gridded dust extinction product, MERRAero captured the observed magnitude and vertical extent of Saharan dust transport, although below 1 km altitude CALIOP reported extinction values that were much greater than those simulated in MERRAero. This result highlighted how essential it is to identify the correct aerosol type (desert dust vs. marine) as subsequent application of a lidar ratio could significantly impact the conversion from backscatter to extinction in instances where the lidar ratio cannot be directly measured. In our comparison to the CALIOP gridded Level 3 product, we demonstrated how the misidentification of marine layers as desert dust can result in higher extinction values for a given backscatter, as the lidar ratio for dust is greater than for marine aerosol.

For our analysis of MERRAero Saharan dust transport using the CALIOP VFM, we outlined two distinct strategies for creating VFMs based on MERRAero simulated quantities. Our first method, the MERRAero-Level 2 method, was an attempt to directly apply the CALIOP VFM algorithm to MERRAero simulated lidar profiles, and required aerosol layer total attenuated backscatter, estimated particulate depolarization ratio and elevation, along with land surface type as inputs. This direct application of the CALIOP VFM is a simulation of how MERRAero quantities map to the CALIOP aerosol types following the CALIOP VFM algorithm logic and can be directly compared to the CALIOP VFM to assess transport biases for individual aerosol species in MERRAero. Our second MERRAero VFM is based on the fundamental outputs of the model, i.e., the speciated extinction, which leads to the so-called MERRAero-Level 3 method. This approach required decisions regarding the prevalence of each individual type for it to be considered significant (e.g., in our case we assumed an aerosol type was significant if it contributed 25 % or more to the total extinction). Our MERRAero-Level 3 VFM can be compared to our MERRAero-Level 2 VFM to evaluate the performance of the CALIOP VFM, which

AMTD
8, 1401–1455, 2015

we demonstrated to have significant implications for the CALIOP extinction product in Fig. 3.

Our comparison of the CALIOP and our MERRAero VFMs for July 2009 yielded several regional differences that have implications for dust transport in MERRAero and understanding limitations of the CALIOP VFM algorithm itself. Over North Africa our MERRAero-Level 2 VFM compared very favorably to the CALIOP VFM by identifying desert dust as the dominant aerosol type, indicating that Saharan dust distributions in MERRAero over North Africa are representative of what is observed by CALIOP. Similarly, our MERRAero VFMs both compared favorably over North Africa and is a region where the CALIOP VFM algorithm performed well. Over the tropical North Atlantic, Caribbean, and East Pacific, our MERRAero-Level 2 VFM compared well with the CALIOP VFM at low altitudes. However, above 1 km, the MERRAero-Level 2 VFM flags a significantly broader Saharan dust plume that extended further to the north, south, and west when compared to the CALIOP Saharan dust plume. Comparing our MERRAero VFMs downwind of the Saharan source region, we found a greater occurrence of desert dust and polluted dust in our MERRAero-Level 2 VFM in regions that were flagged as dust-free in our MERRAero-Level 3 VFM.

Our construction of two MERRAero VFMs led to two major conclusions. Our first conclusion resulted from comparing our MERRAero-Level 2 VFM to the CALIOP VFM. We found an increased prevalence of desert and polluted dust downwind of the Saharan source region in our MERRAero-Level 2 VFM, indicating that MERRAero dust transport is too aggressive. This result demonstrates the utility of using the CALIOP VFM for assessing biases of individual aerosol species in global models, as while our simulated AOTs were comparable to observations in this region, our aerosol speciation was incorrect.

Our second conclusion is that simple application of the CALIOP VFM to drive selection of lidar ratio for extinction retrievals is prone to errors inherent in the retrieval itself. This is illustrated most clearly by comparing our MERRAero-Level 2 and MERRAero-Level 3 VFMs from the MERRAero results (Figs. 7 and 8). Both of these synthetic VFMs

AMTD
8, 1401–1455, 2015

see the same "truth" in the aerosol loading – that is, both are derived from the same aerosol distributions – and in certain areas show very different type identifications. This is most clearly the case over the Gulf of Guinea, west of southern Africa, where the MERRAero-Level 3 method VFM (Fig. 8) identifies elevated smoke layers between the surface and about 4 km, while the MERRAero-Level 2 VFM identifies marine aerosol (Fig. 7). Lidar ratio assigned via these criteria would thus differ by more than a factor of two and so would lead to considerable error in the assigned extinction if the type is misidentified as suggested here. Our second conclusion hints at the future applications of this work. By comparing the MERRAero-Level 2 and MERRAero-Level 3 VFMs we have effectively performed an Observing System Experiment of precisely the kind that will be useful in developing future aerosol satellite missions. The model provides the "nature" state of the Earth system, and the algorithms may be tested against that state to isolate systemic errors in the algorithm. To our knowledge this is the first time this has been done with the CALIOP VFM.

The results of our evaluation are somewhat dependent on how we construct our MERRAero-Level 3 VFM, which is designed to be representative of the actual aerosol types simulated in MERRAero. For the MERRAero-Level 3 VFM, we first must make decisions regarding the mapping of GEOS-5 aerosols and aerosol mixtures to those of CALIOP. For our analysis, we only consider external mixing of aerosols. Internal mixing, could impact the optical properties and lifetime of the aerosol via hygroscopic growth (Adachi et al., 2008) in MERRAero. Additional uncertainty is introduced though our threshold choices for the simulated extinction thresholds used to construct the MERRAero-Level 3 VFM. Adjusting our threshold choice will certainly impact the results of our evaluation, and in this study, a greater threshold requirement could very likely impact the occurrence of desert dust vs. polluted dust over the tropical North Atlantic in our MERRAero-Level 3 VFM. Another potential limitation of our evaluation is related to sampling. In this study, we sampled our simulated MERRAero aerosol distributions across altitudes of aerosol features observed by CALIOP. This limits our ability to identify cases where MERRAero might be simulating aerosols at too high

AMTD
8, 1401–1455, 2015

of an altitude, as our methodology will cap the altitude range to what is observed by CALIOP. However, in order to apply the CALIOP VFM algorithm in the MERRAero-Level 2 method, we must adapt this methodology in order to compute the layer total attenuated backscatter and estimated particulate depolarization ratio for inputs into the CALIOP VFM.

In summary, our analysis illustrates the utility of the CALIOP VFM as a significant tool that may be used to evaluate aerosol transport in global aerosol transport models. From our analysis, we have diagnosed biases in aerosol transport in MERRAero and in the CALIOP VFM algorithm itself, which otherwise would not be possible using column AOT observations alone.

Acknowledgements. We would like to thank the CALIOP team for providing data obtained from the NASA Langley Research Center Atmospheric Science Data Center. Additionally, we would like to thank Brent Holben and Didier Tanr, Victoria Cachorro Revilla, Juan Antuqa Marrero, and Emilio Cuevas Agullo for their efforts in establishing and maintaining the La Parguera, Capo Verde, Camaguey, and Santa Cruz Tenerife AERONET sites. This work was funded by the NASA Postdoctoral Program (NPP) and under support from the Aerosol, Clouds, and Ecosystems (ACE) science working group, supported by Hal Maring.

References

Abdou, W. A., Diner, D. J., Martonchik, V., Bruegge, C. J., Kahn, R. A., Gaitley, B. J., Crean, K. A., Remer, L. A., and Holben, B.: Comparison of coincident MISR and MODIS aerosol optical depths over land and ocean scenes containing AERONET sites, J. Geophys. Res., 110, D02109, doi:10.1029/2008JD010754, 2005.

Adachi, K. and Buseck, P. R.: Internally mixed soot, sulfates, and organic matter in aerosol particles from Mexico City, Atmos. Chem. Phys., 8, 6469–6481, doi:10.5194/acp-8-6469-2008, 2008.

Adams, A. M., Prospero, J. M., and Zhang, C.: CALIPSO-derived three-dimensional structure of aerosol over the Atlantic basin and adjacent continents, J. Climate, 25, 6862–6879, 2012.

AMTD
8, 1401–1455, 2015

Balkanski, Y., Schulz, M., Claquin, T., and Guibert, S.: Reevaluation of Mineral aerosol radiative forcings suggests a better agreement with satellite and AERONET data, Atmos. Chem. Phys., 7, 81–95, doi:10.5194/acp-7-81-2007, 2007.

Benedetti, A., Morcrette, J.-J., Boucher, O., Dethof, A., Engelen, R. J., Fisher, M., Flentje, H., Huneeus, N., Jones, L., Kaiser, J. W., Kinne, S., Mangold, A., Razinger, M., Simmons, A. J., and Suttie, M.: Aerosol analysis and forecast in the European Centre for Medium-Range Weather Forecasts Integrated Forecast System: 2. data assimilation, J. Geophys. Res., 114, D13205, doi:10.1029/2008JD011115, 2009.

Browell, E. V., Ismail, S., Hall, W. M., Moore, S. A., Kooi, S. A., Brackett, V. G., Clayton, M. B., Barrick, J. D. W., Schmidlin, F. J., Higdon, S., Melfi, S. H., and Whiteman, D. N.: LASE validation experiment, in: Advances in Atmospheric Remote Sensing With Lidar, Springer, Berlin Heidelberg, 289–295, 1997.

Buchard, V., da Silva, A. M., Colarco, P., Krotkov, N., Dickerson, R. R., Stehr, J. W., Mount, G., Spinei, E., Arkinson, H. L., and He, H.: Evaluation of GEOS-5 sulfur dioxide simulations during the Frostburg, MD 2010 field campaign, Atmos. Chem. Phys., 14, 1929–1941, doi:10.5194/acp-14-1929-2014, 2014a.

Buchard, V., M. da Silva, A., R. Colarco, P., Darmenov, A., Randles, C. A., Govindaraju, R., Torres, O., Campbell, J., and Spurr, R.: Using the OMI Aerosol Index and Absorption Aerosol Optical Depth to evaluate the NASA MERRA Aerosol Reanalysis, Atmos. Chem. Phys. Discuss., 14, 32177–32231, doi:10.5194/acpd-14-32177-2014, 2014b.

Campbell, J. R., Hlavka, D. L., Welton, E. J., Flynn, C. J., Turner, D. D., Spinhirne, J. D., Scott, V. S., and Hwang, I. H.: Full-time, eye-safe cloud and aerosol lidar observation at atmospheric radiation measurement program sites: instrument and data processing, J. Atmos. Ocean. Tech., 19, 431–442, 2002.

Chen, Z., Torres, O., McCormick, M. P., Smith, W., and Ahn, C.: Comparative study of aerosol and cloud detected by CALIPSO and OMI, Atmos. Environ., 51, 187–195, 2012.

Chin, M., Ginoux, P., Kinne, S., Torres, O., Holben, B. N., Duncan, B. N., Martin, R. V., Logan, J. A., Higurashi, A., and Nakajima, T.: Tropospheric aerosol optical thickness from the GOCART model and comparisons with satellite and sun photometer measurements, J. Atmos. Sci., 59, 461–483, 2002.

Colarco, P. R., Toon, O. B., Torres, O., and Rasch, P. J.: Determining the UV imaginary index of refraction of Saharan dust particles from Total Ozone Mapping Spectrom-

AMTD
8, 1401–1455, 2015

eter data using a three-dimensional model of dust transport, J. Geophys. Res., 107, doi:10.1029/2001JD000903, 2002.
Colarco, P., da Silva, A., Chin, M., and Diehl, T.: Online simulations of global aerosol distributions in the NASA GEOS-4 model and comparisons to satellite and ground-based aerosol optical depth, J. Geophys. Res., 115, D14207, doi:10.1029/2009JD012820, 2010.
Colarco, P. R., Nowottnick, E. P., Randles, C. A., Yi, B., Yang, P., Kim, K.-M., Smith, J. A., and Bardeen, C. G.: Impact of radiatively interactive dust aerosols in the NASA GEO-5 climate model: sensitivity to dust particle shape and refractive index, J. Geophys. Res., 119, 753–786, doi:10.1002/2013JD020046, 2014a.
Colarco, P. R., Kahn, R. A., Remer, L. A., and Levy, R. C.: Impact of satellite viewing-swath width on global and regional aerosol optical thickness statistics and trends, Atmos. Meas. Tech., 7, 2313–2335, doi:10.5194/amt-7-2313-2014, 2014b.
Dee, D. P. and Da Silva, A. M.: Maximum-likelihood estimation of forecast and observation error covariance parameters. Part I: Methodology, Mon. Weather Rev., 127, 1822–1834, 1999.
Dee, D. P., Rukhovets, L., Todling, R., Da Silva, A. M., and Larson, J. W.: An adaptive buddy check for observational quality control, Q. J. Roy. Meteor. Soc., 127, 2451–2471, 2001.
DeMott, P. J., Sassen, K., Poellot, M. R., Baumgardner, D., Rogers, D. C., Brooks, S. D., Prenni, A. J., and Kreidenweis, S. M.: African dust aerosols as atmospheric ice nuclei, Geophys. Res. Lett., 30, 1732, doi:10.1029/2003GL017410, 2003.
Diner, D. J., Beckert, J. C., Reilly, T. H., Brugge, C. J., Conel, J. E., Kahn, R. A., Martonchik, J. V., Ackermann, T. P., Davies, R., Gerstl., S. A. W., Gordon, H. R., Muller, J.-P., Myneni, R. B., Sellers, P. J., Pinty, B., and Verstraete, M. M.: Multi-angle Imaging SpectroRadiometer (MISR) – instrument description and experiment overview, IEEE T. Geosci. Remote, 36, 1072–1087, doi:10.1109/36.700992, 1998.
Dubovik, O., Sinyuk, A., Lapyonok, T., Holben, B. N., Mishchenko, M., Yang, P., Eck, T. F., Volten, H., Munoz, O., Veihelmann, B., van der Zande, W., J., Leon, J.-F., Sorokin, M., and Slutsker, I.: Application of spheroid models to account for aerosol particle nonsphericity in remote sensing of desert dust, J. Geophys. Res.-Atmos., 111, D11208, doi:10.1029/2005JD006619, 2006.
Dunion, J. P. and Velden, C. S.: The impact of the Saharan air layer on Atlantic tropical cyclone activity, B. Am. Meteorol. Soc., 85, 353–365, 2004.

AMTD
8, 1401–1455, 2015

Eck, T. F., Holben, B. N., Reid, J. S., Dubovik, O., Smirnov, A., O'neill, N. T., Slutsker, I., and Kinne, S.: Wavelength dependence of the optical depth of biomass burning, urban, and desert dust aerosols, J. Geophys. Res.-Atmos., 104, 31333–31349, 1999.

Evan, A. T., Dunion, J., Foley, J. A., Heidinger, A. K., and Velden, C. S.: New evidence for a relationship between Atlantic tropical cyclone activity and African dust outbreaks, Geophys. Res. Lett., 33, L19813, doi:10.1029/2006GL026408, 2006.

Freudenthaler, V., Esselborn, M., Wiegner, M., Heese, B., Tesche, M., Ansmann, A., Müller, D. Althausen, D., Wirth, M., Fix, A., Ehret, G., Knippertz, P., Teledano, C., Gasteiger, J., Garhammer, M., and Seefeldner, M.: Depolarization ratio profiling at several wavelengths in pure Saharan dust during SAMUM 2006, Tellus B, 61, 165–179, 2009.

Hagihara, Y., Okamoto, H., and Yoshida, R.: Development of a combined CloudSat-CALIPSO cloud mask to show global cloud distribution, J. Geophys. Res., 115, D00H33, doi:10.1029/2009JD012344, 2010.

Haywood, J., Francis, P., Osborne, S., Glew, M., Loeb, N., Highwood, E, Tanreì, D., Myhre, G., Formenti, P., and Hirst, E.: Radiative properties and direct radiative effect of Saharan dust measured by the C-130 aircraft during SHADE: 1. solar spectrum, J. Geophys. Res., 108, 8577, doi:10.1029/2002JD002687, 2003.

Hess, M., Koepke, P., and Schult, I.: Optical properties of aerosols and clouds: the software package OPAC, B. Am. Meteorol. Soc., 79, 831–844, 1998.

Hill, C., DeLuca, C., Balaji, V., Suarez, M., da Silva, A., and the ESMF Joint Specification Team: The architecture of the Earth system modeling framework, Comput. Sci. Eng., 6, 1–6, 2004.

Holben, B. N., Tanré D., Smirnov, A., Eck, T. F., Slutsker, I., Abuhassan, N., Newcomb, W. W., Schafer, J. S., Chatenet, B., Lavenu, F., Kaufman, Y. J., Vande Castle, J., Setzer, A., Markham, B., Clark, D., Frouin, R., Halthore, R., Karneli, A., O'Neill, N. T., Pietra, C., Pinker, R. T., Voss, K., and Zibordi, G.: An emerging ground-based aerosol climatology: aerosol optical depth from AERONET, J. Geophys. Res., 106, 12067–12097, 2001.

Huang, H., Huang, J., Bi, J., Wang, G., Wang, W., Fu, Q., Li, Z., Tsay, S. C., and Shi, J.: Dust aerosol vertical structure measurements using three MPL lidars during 2008 China–US joint dust field experiment, J. Geophys. Res., 115, D00K15, doi:10.1029/2009JD013273, 2010.

Huneeus, N., Schulz, M., Balkanski, Y., Griesfeller, J., Prospero, J., Kinne, S., Bauer, S., Boucher, O., Chin, M., Dentener, F., Diehl, T., Easter, R., Fillmore, D., Ghan, S., Ginoux, P., Grini, A., Horowitz, L., Koch, D., Krol, M. C., Landing, W., Liu, X., Mahowald, N., Miller, R., Morcrette, J.-J., Myhre, G., Penner, J., Perlwitz, J., Stier, P., Takemura, T., and Zender, C. S.:

AMTD
8, 1401–1455, 2015

Global dust model intercomparison in AeroCom phase I, Atmos. Chem. Phys., 11, 7781–7816, doi:10.5194/acp-11-7781-2011, 2011.
Intergovernmental Panel on Climate Change: Climate Change 2013, the Physical Science Basis: Working Group I Contribution to the IPCC Fifth Assessment Report, Cambridge University Press, 2014.
Jenkins, G. S., Pratt, A. S., and Heymsfield, A.: Possible linkages between Saharan dust and tropical cyclone rain band invigoration in the eastern Atlantic during NAMMA-06, Geophys. Res. Lett., 35, L08815, doi:10.1029/2008GL034072, 2008.
Jickells, T. D., An, Z. S., Andersen, K. K., Baker, A. R., Bergametti, G., Brooks, N., Cao, J. J., Boyd, P. W., Duce, R. A., Hunter, K. A., Kawahata, H., Kubilay, N., laRoche, J., Liss, P. S., Mahowald, N., Prospero, J. M., Ridgwell, A. J., Tegen, I., and Torres, R. : Global iron connections between desert dust, ocean biogeochemistry, and climate, Science, 308, 67–71, 2005.
Kahn, R. A., Li, W.-H., Martonchik, J. V., Bruegge, C. J., Diner, D. J., Gaitley, B. J., and Abdou, W.: MISR calibration and implications for low-light-level aerosol retrieval over dark water, J. Atmos. Sci., 62, 1032–1052, 2005.
Kaufman, Y. J., Tanré, D., Remer, D. L., Vermote, E. F., Chu, A., and Holben, B. N.: Operational remote sensing of tropospheric aerosol over land from EOS moderate resolution imaging spectroradiometer, J. Geophys. Res., 102, 17051–17067, 1997.
Kessner, A. L., Wang, J., Levy, R. C., and Colarco, P. R.: Remote sensing of surface visibility from space: a look at the United States East Coast, Atmos. Environ., 81, 136–147, doi:10.1016/j.atmosenv.2013.08.050, 2013.
Kim, D., Chin, M., Yu, H., Eck, T. F., Sinyuk, A., Smirnov, A., and Holben, B. N.: Dust optical properties over North Africa and Arabian Peninsula derived from the AERONET dataset, Atmos. Chem. Phys., 11, 10733–10741, doi:10.5194/acp-11-10733-2011, 2011.
Kim, D., Chin, M., Yu, H., Diehl, T., Tan, Q., Kahn, R. A., Tsigaridis, K., Bauer, S. E., Takemura, T., Pozzoli, L, Bellouin, N., Schulz, M., Peyridieu, S., Chédin, A., and Koffi, B.: Sources, sinks, and transatlantic transport of North African dust aerosol: a multimodel analysis and comparison with remote sensing data, J. Geophys. Res.-Atmos., 119, 6259–6277, doi:10.1002/2013JD021099, 2014.
Kinne, S., Schulz, M., Textor, C., Guibert, S., Balkanski, Y., Bauer, S. E., Berntsen, T., Berglen, T. F., Boucher, O., Chin, M., Collins, W., Dentener, F., Diehl, T., Easter, R., Feichter, J., Fillmore, D., Ghan, S., Ginoux, P., Gong, S., Grini, A., Hendricks, J., Herzog, M.,

AMTD
8, 1401–1455, 2015

Horowitz, L., Isaksen, I., Iversen, T., Kirkevåg, A., Kloster, S., Koch, D., Kristjansson, J. E., Krol, M., Lauer, A., Lamarque, J. F., Lesins, G., Liu, X., Lohmann, U., Montanaro, V., Myhre, G., Penner, J., Pitari, G., Reddy, S., Seland, O., Stier, P., Takemura, T., and Tie, X.: An AeroCom initial assessment – optical properties in aerosol component modules of global models, Atmos. Chem. Phys., 6, 1815–1834, doi:10.5194/acp-6-1815-2006, 2006.

Koehler, K. A., Kreidenweis, S. M., DeMott, P. J., Petters, M. D., Prenni, A. J., and Möhler, O.: Laboratory investigations of the impact of mineral dust aerosol on cold cloud formation, Atmos. Chem. Phys., 10, 11955–11968, doi:10.5194/acp-10-11955-2010, 2010.

Kumar, P., Nenes, A., and Sokolik, I. N.: The importance of absorption for CCN activity and hygroscopic properties of mineral dust aerosols, Geophys. Res. Lett., 36, L24804, doi:10.1029/2009GL040827, 2009.

Lary, D. J., Nikitkov, A., and Stone, D. N.: Which Machine-Learning Models Best Predict Online Auction Seller Deception Risk? 2010 American Accounting Association AAA Strategic and Emerging Technologies, 2010.

Lau, W. K. and Kim, K. M.: Cooling of the Atlantic by Saharan dust, Geophys. Res. Lett., 34, L23811, doi:10.1029/2007GL031538, 2007.

L'Ecuyer, T. S. and Jiang, J.: Touring the atmosphere aboard the a-train, Phys. Today, 63, 36–41, 2010.

Levy, R. C., Remer, L. A., and Dubovik, O.: Global aerosol optical properties and application to moderate resolution imaging spectroradiometer aerosol retrieval over land, J. Geophys. Res., 112, D13210, doi:10.1029/2006JD007815, 2007a.

Levy, R. C., Remer, L. A., Mattoo, S., Vermote, E. F., and Kaufman, Y. K.: Second-generation operational algorithm: retrieval of aerosol properties over land from inversion of moderate resolution imaging spectroradiometer spectral reflectance, J. Geophys. Res., 112, D13211, doi:10.1029/2006JD007811, 2007b.

Liu, Z., Omar, A. H., Hu, Y., Vaughan, M. A., Winker, D. M., Poole, L. R., and Kovacs, T. A.: CALIOP Algorithm Theoretical Basis Document, Part 3: Scene Classification Algorithms, NASA-CNES document PC-SCI-203, 2005.

Liu, Z., Omar, A., Vaughan, M., Hair, J., Kittaka, C., Hu, Y., Powell, K., Trepte, C., Winker, D., Hostetler, C., Ferrare, R., and Pierce, R.: CALIPSO lidar observations of the optical properties of Saharan dust: a case study of longrange transport, J. Geophys. Res.-Atmos., 113, D07207, doi:10.1029/2007JD008878, 2008.

AMTD
8, 1401–1455, 2015

Loveland, T. R., Reed, B. C., Brown, J. F., Ohlen, D. O., Zhu, Z., Yang, L. W. M. J., and Merchant, J. W.: Development of a global land cover characteristics database and IGBP DISCover from 1 km AVHRR data, Int. J. Remote Sens., 21, 1303–1330, 2000.

Mahowald, N. M., Engelstaedter, S., Lou, C., Sealy, A., Artaxo, P., Benitez-Nelson, C., Connet, S., Chen, Y., Chuang, P. Y., Cohen, D. D., Dulac, F., Herut, B., Johansen, A. M., Kubilay, N., Losno, R., Maenhaut, W., Paytan, A., Prospero, J. M., Shank, L. M., and Siefert, R. L.: Atmospheric iron deposition: global distribution, variability, and human perturbations, Annual Review of Marine Science, 1, 245–278, doi:10.1146/annurev.marine.010908.163727, 2009.

McGill, M. J., Hlavka, D. L., Hart, W. D., Spinhirne, J. D., Scott, V. S., and Schmid, B.: The cloud physics lidar: instrument description and initial measurement results, Appl. Optics, 41, 3725–3734, 2002.

Meng, Z., Yang, P., Kattawar, G. W., Bi, L., Liou, K. N., and Laszlo, I.: Single-scattering properties of tri-axial ellipsoidal mineral dust aerosols: a database for application to radiative transfer calculations, J. Aerosol Sci., 41, 501–512, 2010.

Miller, R. L., Tegen, I., and Perlwitz, J.: Surface radiative forcing of soil dust aerosols and the hydrologic cycle, J. Geophys. Res., 109, D04203, doi:10.1029/2003JD004085, 2004.

Mishchenko, M. I., Liu, L., and Mackowski, D. W.: *T* matrix modeling of linear depolarization by morphologically complex soot and soot-containing aerosols, J. Quant. Spectrosc. Ra., 123, 135–144, doi:10.1016/j.jqsrt.2012.11.012, 2013.

Nowottnick, E., Colarco, P., Ferrare, R., Chen, G., Ismail, S., Anderson, B., and Browell, E.: Online simulations of mineral dust aerosol distributions: comparisons to NAMMA observations and sensitivity to dust emission parameterization, J. Geophys. Res.-Atmos., 115, D03202, doi:10.1029/2009JD012692, 2010.

Nowottnick, E., Colarco, P., da Silva, A., Hlavka, D., and McGill, M.: The fate of saharan dust across the atlantic and implications for a central american dust barrier, Atmos. Chem. Phys., 11, 8415–8431, doi:10.5194/acp-11-8415-2011, 2011.

Omar, A. H., Won, J. G., Winker, D. M., Yoon, S. C., Dubovik, O., and McCormick, M. P.: Development of global aerosol models using cluster analysis of Aerosol Robotic Network (AERONET) measurements, J. Geophys. Res.-Atmos., 110, D10S14, doi:10.1029/2004JD004874, 2005.

Omar, A. H., Winker, D. M., Kittaka, C., Vaughan, M. A., Liu, Z., Hu, Y., and Hostetler, C. A.: The CALIPSO automated aerosol classification and lidar ratio selection algorithm, J. Atmos. Ocean. Tech., 26, 1994–2014, doi:10.1175/2009JTECHA1231.1, 2009.

AMTD
8, 1401–1455, 2015

Pawson, S., Stolarski, R. S., Douglass, A. R., Newman, P. A., Nielsen, J. E., Frith, S. M., and Gupta, M. L.: Goddard Earth Observing System chemistry–climate model simulations of stratospheric ozone–temperature coupling between 1950 and 2005, J. Geophys. Res., 113, D12103, doi:10.1029/2007JD009511, 2008.

Putman, W. M. and Suarez, M.: Cloud-system resolving simulations with the NASA Goddard Earth Observing System global atmospheric model (GEOS-5), Geophys. Res. Lett., 38, L16809, doi:10.1029/2011GL048438, 2011.

Reale, O., Lau, W.-K., Kim, K.-M., and Brin, E.: Atlantic tropical cyclogenetic processes during SOP-3 NAMMA in the GEOS-5 global data assimilation and forecast system, J. Atmos. Sci., 66, 3563–3578, doi:10.1175/2009JAS3123.1, 2009.

Reid, J. S., Kinney, J. E., Westphal, D. L., Holben, B. N., Welton, E. J., Tsay, S.-C., Eleuterio, D. P., Campbell, J. R., Christopher, S. A., Colarco, P. R., Jonsson, H. H., Livingston J. M., Maring, H. B., Meier, M. L., Pilewskie, P., Prospero, J. M., Reid, E. A., Remer, L. A., Russell, P. B., Savoie, D. L., Smirnow, A., and Tanré, D. : Analysis of measurements of Saharan dust by airborne and ground-based remote sensing methods during the Puerto Rico Dust Experiment (PRIDE), J. Geophys. Res., 108, 8586, doi:10.1029/2002JD002493, 2003.

Remer, L. A., Kaufman, Y. J., Tanré, D., Mattoo, S., Chu, D. A., Martins, J. V., Li, R.-R., Ichoku, C., Levy, R. C., Kleidman, R. G., Eck, T. F., Vermote, E., and Holben, B. N.: The MODIS aerosol algorithm, products, and validation, J. Atmos. Sci., 62, 947–973, 2005.

Rienecker, M. M., Suarez, M. J., Todling, R., Bacmeister, J., Takacs, L., Liu, H.-C., Gu, W., Sienkiewicz, M., Koster, R. D., Gelaro, R., Stajner, I., and Nielsen, J. E.: The GEOS-5 Data Assimilation System-Documentation of Versions 5.0.1, 5.1.0, and 5.2.0. Technical Report Series on Global Modeling and Data Assimilation 104606, 27 pp., 2008.

Reinecker, M. M., Suarez, M. J., Gelaro, R., Todling, R., Bacmeister, J., Liu, E., Bosilovich, M. G., Schubert, S. D., Takacs, L., Kim, G.-K., Bloom, S., Chen, J., Collins, D., Conaty, A., da Silva, A., Gu, W., Joiner, J., Koster, R. D., Lucchesi, R., Molod, A., Owens, T., Pawson, S., Pegion, P., Redder, C. R., Reichle, R., Robertson, F. R., Ruddick, A. G., Sienkiewicz, M., and Woollen, J.: MERRA – NASA's Modern-Era Retrospective Analysis for Research and Applications, J. Climate, 24, 3624–3648, doi:10.1175/JCLI-D-11-00015.1, 2011.

Rogers, R. R., Hair, J. W., Hostetler, C. A., Ferrare, R. A., Obland, M. D., Cook, A. L., Harper, D. B., Burton, S. P., Shinozuka, Y., McNaughton, C. S., Clarke, A. D., Redemann, J., Russell, P. B., Livingston, J. M., and Kleinman, L. I.: NASA LaRC airborne high spectral res-

AMTD
8, 1401–1455, 2015

olution lidar aerosol measurements during MILAGRO: observations and validation, Atmos. Chem. Phys., 9, 4811–4826, doi:10.5194/acp-9-4811-2009, 2009.
Rosenfeld, D., Rudich, Y., and Lahav, R.: Desert dust suppressing precipication: A possible desertification loop, P. Natl. Acad. Sci. USA, 98, 5975–5980, 2001.
Russell, P. B., Livingston, J. M., Dutton, E. G., Pueschel, R. F., Reagan, J. A., DeFoor T. E., Box, M. A., Allen, D., Pilewskie, P., Herman, B. M., Kinne, S. A., and Hofmann, D. J.: Pinatubo and pre-Pinatubo optical-depth spectra: Mauna Loa measurements, comparisons, inferred particle size distributions, radiative effects, and relationship to lidar data, J. Geophys. Res.-Atmos., 98, 22969–22985, 1993.
Ryder, C. L., Highwood, E. J., Rosenberg, P. D., Trembath, J., Brooke, J. K., Bart, M., Dean, A., Crosier, J., Dorsey, J., Brindley, H., Banks, J., Marsham, J. H., McQuaid, J. B., Sodemann, H., and Washington, R.: Optical properties of Saharan dust aerosol and contribution from the coarse mode as measured during the Fennec 2011 aircraft campaign, Atmos. Chem. Phys., 13, 303–325, doi:10.5194/acp-13-303-2013, 2013.
Sessions, W. R., Reid, J. S., Benedetti, A., Colarco, P. R., da Silva, A., Lu, S., Sekiyama, T., Tanaka, T. Y., Baldasano, J. M., Basart, S., Brooks, M. E., Eck, T. F., Iredell, M., Hansen, J. A., Jorba, O. C., Juang, H.-M. H., Lynch, P., Morcrette, J.-J., Moorthi, S., Mulcahy, J., Pradhan, Y., Razinger, M., Sampson, C. B., Wang, J., and Westphal, D. L.: Development towards a global operational aerosol consensus: basic climatological characteristics of the International Co-operative for Aerosol Prediction Multi-Model Ensemble (ICAP-MME), Atmos. Chem. Phys. Discuss., 14, 14933–14998, doi:10.5194/acpd-14-14933-2014, 2014.
Shi, Y., Zhang, J., Reid, J. S., Liu, B., and Hyer, E. J.: Critical evaluation of cloud contamination in the MISR aerosol products using MODIS cloud mask products, Atmos. Meas. Tech., 7, 1791–1801, doi:10.5194/amt-7-1791-2014, 2014.
Smirnov, A., Holben, B. N., Eck, T. F., Dubovik, O., and Slutsker, I.: Cloud-screening and quality control algorithms for the AERONET database, Remote Sens. Environ., 73, 337–349, 2000.
Sokolik, I. N. and Toon, O. B.: Direct radiative forcing by anthropogenic airborne mineral aerosols, Nature, 381, 681–683, 1996.
Swap, R., Garstang, M., Greco, S., Talbot, R., and Kallberg, P.: Saharan dust in the Amazon Basin, Tellus B, 44, 133–149, doi:10.1034/j.1600-0889.1992.t01-1-00005.x, 1992.
Tanré, D., Kaufman, Y. J., Herman, M., and Mattoo, S.: Remote sensing of aerosol properties over oceans using the MODIS/EOS spectral radiances, J. Geophys. Res.-Atmos., 102, 16971–16988, 1997.

AMTD
8, 1401–1455, 2015

Tegen, I. and Miller, R.: A general circulation model study on the interannual variability of soil dust aerosol, J. Geophys. Res., 103, 25975–25995, 1998.

Textor, C., Schulz, M., Guibert, S., Kinne, S., Balkanski, Y., Bauer, S., Berntsen, T., Berglen, T., Boucher, O., Chin, M., Dentener, F., Diehl, T., Easter, R., Feichter, H., Fillmore, D., Ghan, S., Ginoux, P., Gong, S., Grini, A., Hendricks, J., Horowitz, L., Huang, P., Isaksen, I., Iversen, I., Kloster, S., Koch, D., Kirkevåg, A., Kristjansson, J. E., Krol, M., Lauer, A., Lamarque, J. F., Liu, X., Montanaro, V., Myhre, G., Penner, J., Pitari, G., Reddy, S., Seland, Ø., Stier, P., Takemura, T., and Tie, X.: Analysis and quantification of the diversities of aerosol life cycles within AeroCom, Atmos. Chem. Phys., 6, 1777–1813, doi:10.5194/acp-6-1777-2006, 2006.

Vaughan, M. A., Winker, D. M., and Powell, K. A.: CALIOP algorithm theoretical basis document, Part 2: Feature detection and layer properties algorithms, Rep. PC-SCI, 202, 87, 2005.

Welton, E. J., Voss, K. J., Gordon, H. R., Maring, H., Smirnov, A., Holben, B., Schmid, B., Livingston, J. M., Russell, P. B., Durkee, P. A., Formenti, P., and Andreae, M. O.: Ground-based lidar measurements of aerosols during ACE-2: instrument description, results, and comparisons with other ground-based and airborne measurements, Tellus B, 52, 635–650, 2000.

Welton, E. J., Campbell, J. R., Spinhirne, J. D., and Scott, V. S.: Global monitoring of clouds and aerosols using a network of micro-pulse lidar systems, in: Lidar Remote Sensing for Industry and Environmental Monitoring, edited by: Singh, U. N., Itabe, T., and Sugimoto, N., Proc. SPIE, 4153, 151–158, 2001.

Winker, D. M.: Accounting for multiple scattering in retrievals from space lidar, in: Lidar Multiple Scattering Experiments, International Society for Optics and Photonics, 128–139, 2003.

Winker, D. M., Hostetler, C. A., Vaughan, M. A., and Omar, A. H.: CALIOP algorithm theoretical basis document, Part 1: CALIOP instrument, and algorithms overview, Release, 2, 29 pp., 2006.

Winker, D. M., Vaughan, M. A., Omar, A., Hu, Y., and Powell, K. A.: Overview of the CALIPSO mission and CALIOP data processing algorithms, J. Atmos. Ocean. Tech., 26, 2310–2323, 2009.

Winker, D. M., Tackett, J. L., Getzewich, B. J., Liu, Z., Vaughan, M. A., and Rogers, R. R.: The global 3-D distribution of tropospheric aerosols as characterized by CALIOP, Atmos. Chem. Phys., 13, 3345–3361, doi:10.5194/acp-13-3345-2013, 2013.

AMTD
8, 1401–1455, 2015

Yasunari, T. J., Colarco, P. R., Lau, K.-M., Osada, K., Kido, M., Mahanama, S. P. P., Kim, K.-M., and da Silva, A. M.: Total dust deposition during preciptiation in Toyama, Japan, in the Spring 2009: a sensitivity analysis with the NASA GEOS-5 model, Atmos. Res., submitted, 2014.

Yoshioka, M., Mahowald, N. M., Conley, A. J., Collins, W. D., Fillmore, D. W., Zender, C. S., and Coleman, D. B.: Impact of desert dust radiative forcing on Sahel precipitation: relative importance of dust compared to sea surface temperature variations, vegetation changes, and greenhouse gas warming, J. Climate, 20, 1445–1467, 2007.

Yoshida, R., Okamoto, H., Hagihara, Y., and Ishimoto, H.: Global analysis of cloud phase and ice crystal orientation from Cloud Aerosol Lidar and Infrared Pathfinder Satellite Observation (CALIPSO) data using attenuated backscattering and depolarization ratio, J. Geophys. Res., 115, D00H32, doi:10.1029/2009JD012334, 2010.

Zhang, J. and Reid, J. S.: MODIS aerosol product analysis for data assimilation: assessment of overocean level 2 aerosol optical thickness retrievals, J. Geophys. Res.-Atmos., 111, D22207, doi:10.1029/2005JD006898, 2006.

Zhang, J., Reid, J. S., Westphal, D. L., Baker, N. L., and Hyer, E, J.: A system for operational aerosol optical depth data assimilation over global oceans, J. Geophys. Res., 113, D10208, doi:10.1029/2007JD009065, 2008.

Zhu, A., Ramanathan, V., Li, F., and Kim, D.: Dust plumes over the Pacific, Indian, and Atlantic oceans: climatology and radiative impact, J. Geophys. Res., 112, D16208, doi:10.1029/2007JD008427, 2007.

AMTD
8, 1401–1455, 2015

Table 1. CALIOP VFM mapping algorithm presented in table form. We refer for Omar et al. (2009) for an algorithm flowchart. "–" indicates that the property of an aerosol layer is not considered in assigning aerosol type.

Pathway	Land Surface Type	Attenuated Backscatter [$km^{-1}\,sr^{-1}$]	Depolarization Ratio	Elevated Layer	Aerosol Type
1	Snow or Ice	$\gamma > 0.0015$	–	–	Clean Continental (C)
2	Snow or Ice	$\gamma < 0.0015$	–	–	Polluted Continental (PC)
3	Land or Ocean	–	$0.075 < \delta < 0.20$	–	Polluted Dust (PD)
4	Land or Ocean	–	$\delta > 0.20$	–	Desert Dust (DU)
5	Land (Desert)	$\gamma < 0.0005$	$\delta < 0.075$	–	Polluted Dust (PD)
6	Land (Non-Desert)	$\gamma < 0.0005$	$\delta < 0.075$	–	Clean Continental (C)
7	Land	$\gamma > 0.0005$	$\delta < 0.075$	No	Polluted Continental (PC)
8	Ocean	$\gamma < 0.01$	$\delta > 0.05$	–	Polluted Continental (PC)
9	Ocean	$\gamma < 0.01$	$\delta < 0.05$	No	Marine (M)
10	Ocean	$\gamma > 0.01$	$\delta < 0.075$	No	Marine (M)
11	Land	$\gamma > 0.0005$	$\delta < 0.075$	Yes	Smoke (SM)
12	Ocean	–	$\delta < 0.075$	Yes	Smoke (SM)

AMTD
8, 1401–1455, 2015

Table 2. Mapping of MERRAero aerosol mixtures to CALIOP VFM flags.

CALIPSO and MERRAero Aerosol VFM Types	MERRAero Level 3 Aerosol Mixtures	MERRAero Level 3 Minimum Aerosol Fractions for Typing
No Signal or Cloud	N/A	N/A
Marine (M)	Sea Salt	$F_{ss} \geq 0.75$
Desert Dust (DU)	Dust	$F_{du} \geq 0.75$
Polluted Continental (PC)	Sulfate + Carbon	$F_{su}, F_c \geq 0.25, F_{su} + F_c \geq 0.75$
Clean Continental (C)	Sulfate	$F_{su} \geq 0.75$
Polluted Dust (PD)	Dust + Sulfate	$F_{du}, F_{su} \geq 0.25, F_{du} + F_{su} \geq 0.75$
	Dust + Carbon	$F_{du}, F_c \geq 0.25, F_{du} + F_c \geq 0.75$
	Dust + Sulfate + Carbon	$F_{du}, F_{su}, F_c \geq 0.25, F_{du} + F_{su} + F_c \geq 0.75$
	Dust + Sea Salt	$F_{du}, F_{ss} \geq 0.25, F_{du} + F_{ss} \geq 0.75$
	Dust + Sulfate + Sea Salt	$F_{du}, F_{su}, F_{ss} \geq 0.25, F_{du} + F_{su} + F_{ss} \geq 0.75$
	Dust + Carbon + Sea Salt	$F_{du}, F_c, F_{ss} \geq 0.25, F_{du} + F_c + F_{ss} \geq 0.75$
Smoke (SM)	Carbon	$F_c \geq 0.75$
N/A	Sea Salt + Carbon	$F_{ss}, F_c \geq 0.25, F_{ss} + F_c \geq 0.75$
	Sea Salt + Sulfate	$F_{ss}, F_{su} \geq 0.25, F_{ss} + F_{su} \geq 0.75$

AMTD
8, 1401–1455, 2015

Table 3. MERRAero-Level 3 and Mie theory computed CALIOP 532 lidar ratio (S_a) and single scattering albedo (SSA) for each VFM aerosol type.

CALIPSO and MERRAero Aerosol VFM Types	MERRAero 532 nm S_a	Computed CALIOP 532 nm S_a	MERRAero 532 nm SSA	Computed CALIOP 532 nm SSA
Marine (M)	32	25	0.98	0.99
Desert Dust (DU)	46	40	0.92	0.92
Polluted Continental (PC)	61	69	0.89	0.93
Clean Continental (C)	63	34	0.92	0.90
Polluted Dust (PD)	49	60	0.92	0.85
Smoke (SM)	59	75	0.86	0.83

AMTD
8, 1401–1455, 2015

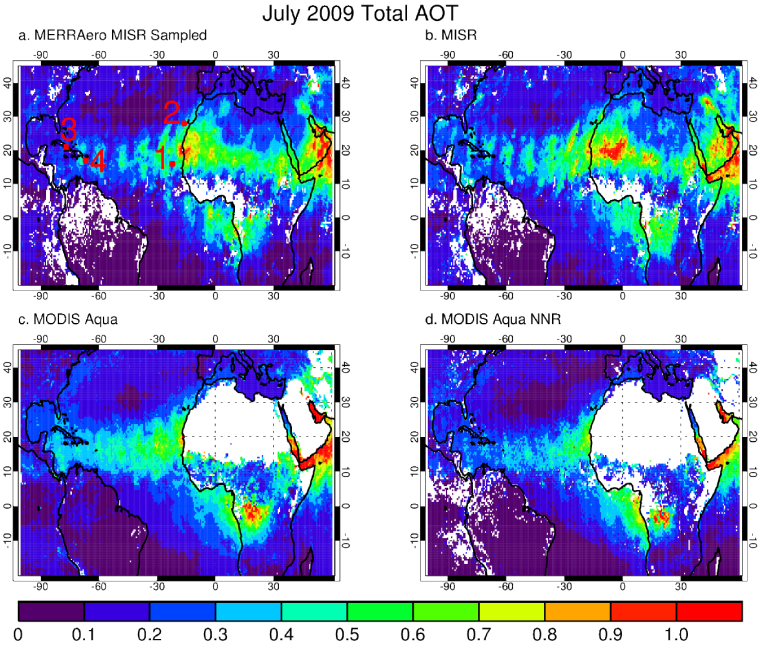

Figure 1. July 2009 AOT for MERRAero sampled along MISR track **(a)**, MISR **(b)**, MODIS-Aqua standard retrieval **(c)**, and MODIS-Aqua NNR **(d)** with AERONET locations overlaid (1 – Capo Verde, 2 – Santa Cruz Tenerife, 3 – Camaguey and 4 – La Parguera). White areas correspond to regions where no aerosol retrievals were made.

AMTD
8, 1401–1455, 2015

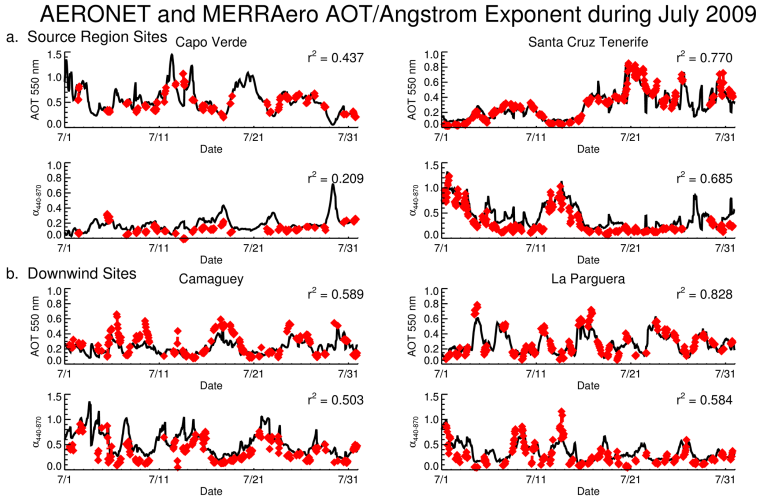

Figure 2. AERONET (red) comparisons to MERRAero (black) AOT and Angstrom Exponent at sites near the source region **(a)** and downwind in the Caribbean **(b)**.

AMTD
8, 1401–1455, 2015

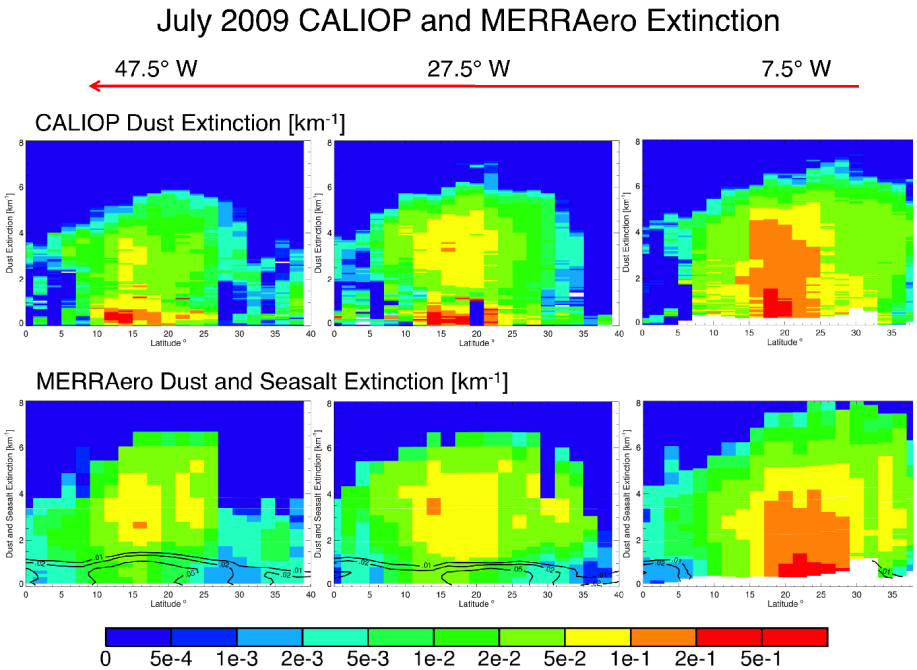

Figure 3. July 2009 CALIOP (top) dust and MERRAero (bottom) dust and seasalt (contour) Level 3 extinction at several north–south slices at longitudes 47.5° W, 27.5° W, and 7.5° W.

AMTD
8, 1401–1455, 2015

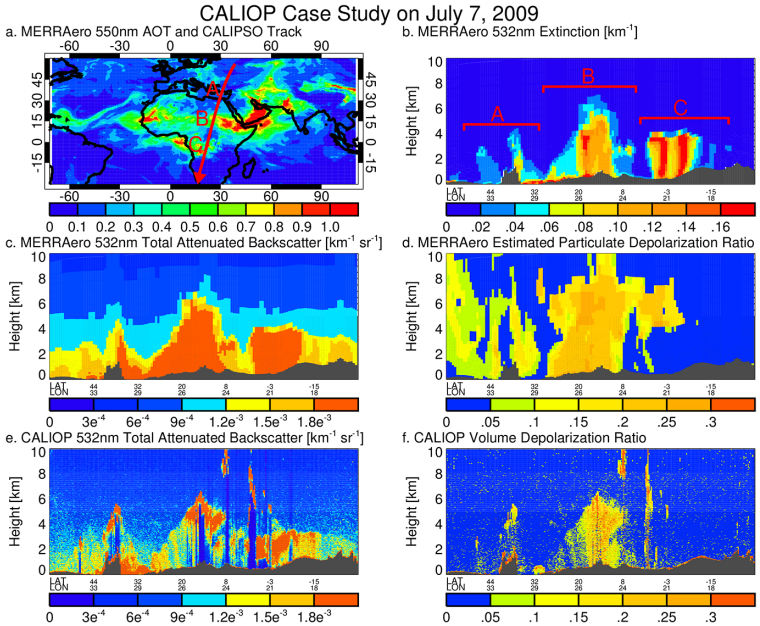

Figure 4. (a) MERRAero 550 nm total AOT at 00Z and CALIPSO track from 00Z–01Z over 3 different aerosol regimes, **(b)** MERRAero 532 nm total extinction, **(c)** MERRAero 532 nm total attenuated backscatter, **(d)** MERRAero estimated particulate depolarization ratio, **(e)** CALIOP 532 nm total attenuated backscatter, and **(f)** CALIOP depolarization ratio on 7 July 2009.

AMTD
8, 1401–1455, 2015

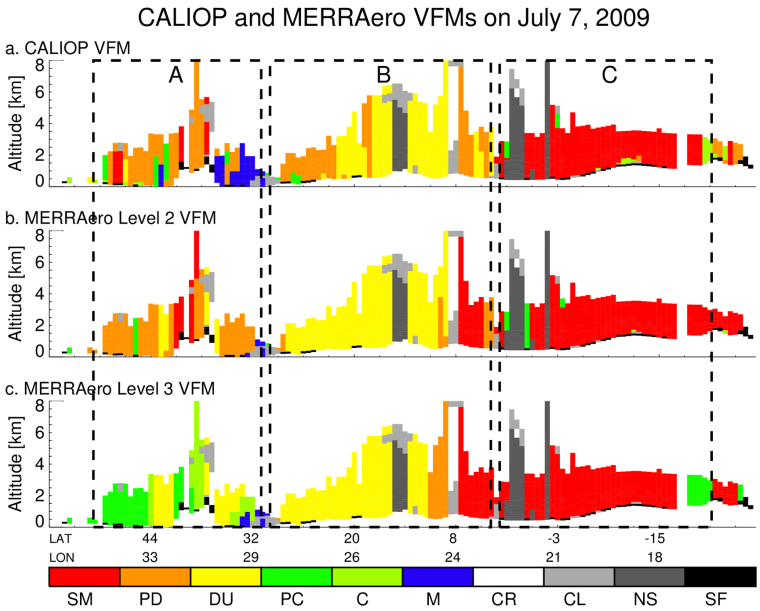

Figure 5. (a) CALIOP VFM, **(b)** MERRAero-Level 2 VFM, and **(c)** MERRAero-Level 3 on 7 July 2009. Aerosol types include smoke (SM), polluted dust (PD), desert dust (DU), clean continental (C), and marine (M). Regions free of aerosol and clouds are classified as clear (CR). Clouds (CL) and associated signal attenuation (NS), as well as the surface (SF) are also shown.

AMTD
8, 1401–1455, 2015

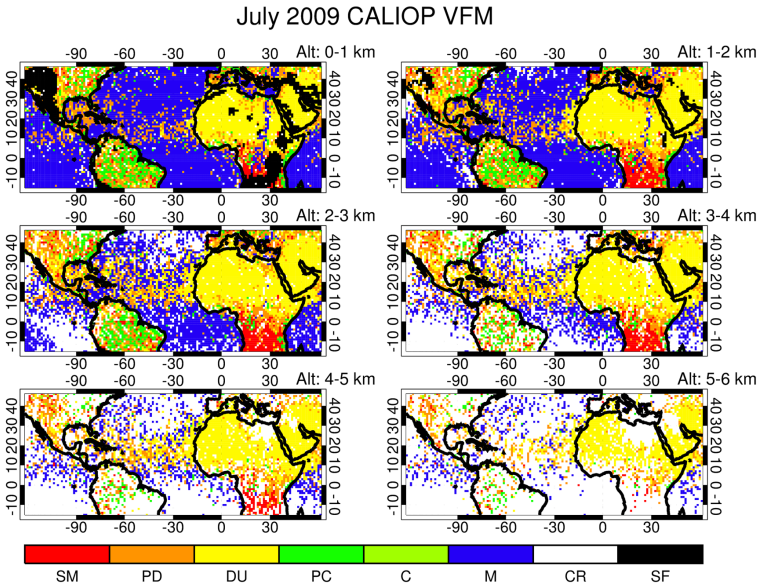

Figure 6. CALIOP VFM at 1 km intervals for July 2009. Aerosol types include smoke (SM), polluted dust (PD), desert dust (DU), clean continental (C), and marine (M). Regions free of aerosol and clouds (CR), as well as the surface (SF) are also shown.

AMTD
8, 1401–1455, 2015

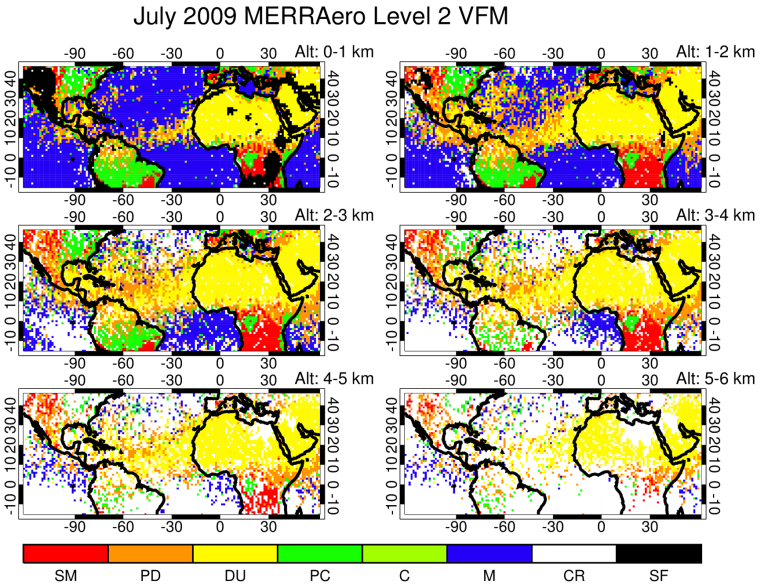

Figure 7. MERRAero-Level 2 VFM at 1 km intervals for July 2009. Aerosol types include smoke (SM), polluted dust (PD), desert dust (DU), clean continental (C), and marine (M). Regions free of aerosol and clouds (CR), as well as the surface (SF) are also shown.

AMTD
8, 1401–1455, 2015

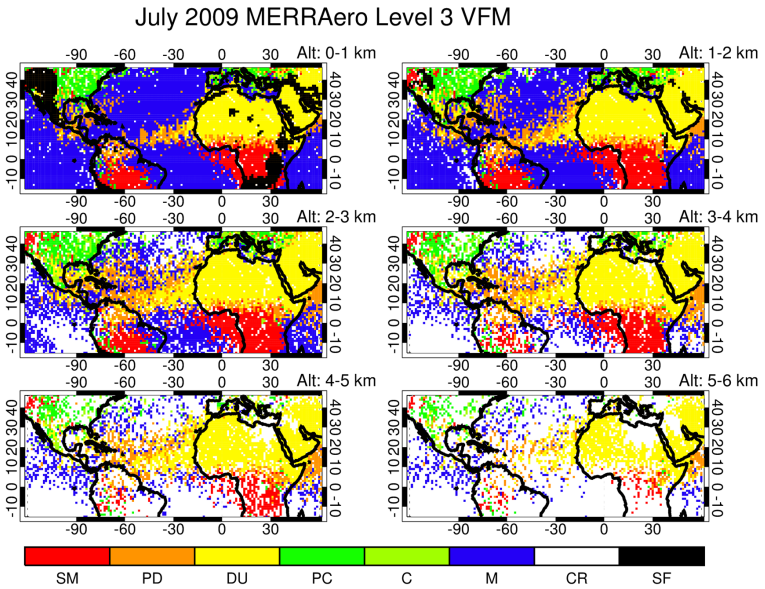

Figure 8. MERRAero-Level 3 VFM at 1 km intervals for July 2009. Aerosol types include smoke (SM), polluted dust (PD), desert dust (DU), clean continental (C), and marine (M). Regions free of aerosol and clouds (CR), as well as the surface (SF) are also shown.

AMTD
8, 1401–1455, 2015

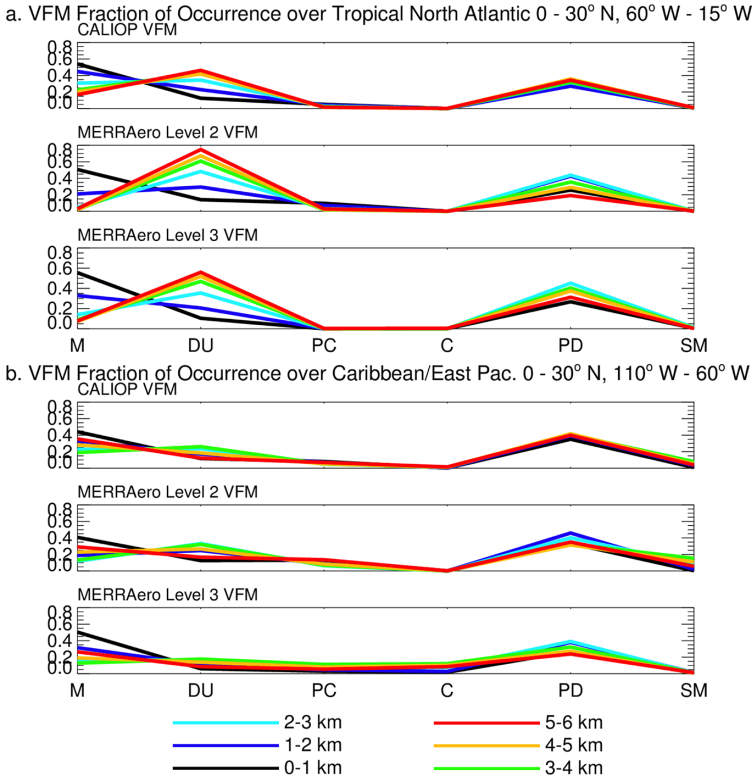

Figure 9. VFM fraction of occurrence over the tropical North Atlantic **(a)** and Caribbean/Eastern Pacific **(b)**. Aerosol types include marine (M), desert dust (DU), polluted continental (PC), clean continental (C), polluted dust (PD), and smoke (SM).

AMTD
8, 1401–1455, 2015